Defence Research and Development Canada
Recherche et développement pour la défense Canada

DEFENCE R&D DÉFENSE

# An Approximate Method for Modelling Laser Light Scattering from Biological Cells

Shao, Y. and Yee, E.
Defence R&D Canada – Suffield

**Addendum**

In error, the original report (DRDC Suffield TR 2004-187, October 2004 "An Approximate Method for Modelling Laser Light Scattering from Biological Cells") did not indicate that the described methodology was first reported in the following publication: Shao, Y., Maximov, A.V., Ourdev, I.G., Rozmus, W., and Capjack, C.E. (2001) "Spectral Method Simulations of Light Scattering by Biological Cells", IEEE Journal of Quantum Electronics, 37(5), 617-625.

Technical Report
DRDC Suffield TR 2004-187
October 2004

Canada

# An Approximate Method for Modelling Laser Light Scattering from Biological Cells

Shao, Y. and Yee, E.
Defence R&D Canada – Suffield

**Defence R&D Canada – Suffield**

Technical Report

DRDC Suffield TR 2004-187

October 2004

Author

Y. Shao

Approved by

Dr J. Lavigne
Head, Chemical and Biological Section

Approved for release by

Dr R. Bide
Chair, DRDC Suffield DRP

# Abstract

A new technique for approximating the scattering of laser light by biological cells is reported. This technique is based on a three-dimensional scalar wave equation approximation of the full Maxwell's field equations for the electromagnetic field. This scalar wave equation for describing the light scattering patterns of cells containing arbitrary morphological structure (e.g., various organelles) is solved numerically using a spectral method. The accuracy of the spectral numerical method is verified by comparison with solutions obtained from linear perturbation theory and Mie theory. Comparison with Mie theory shows that the three-dimensional scalar wave equation is a good approximation to the full Maxwell's field equations for light scattering up to moderate forward scattering angles (i.e., for scattering angles less than about 35°). The approximate technique used here is capable of correctly predicting the scattered intensity patterns from biological cells over a dynamic range spanning six orders of magnitude. The new technique can be applied to calculate the light scattering either from an individual biological cell and from a sample containing an ensemble of such biological cells. The scattering intensity patterns predicted using the new technique can potentially be applied to diagnose the size and internal structure of biological cells, making it a valuable interpretative tool in flow cytometry (e.g., in the detection of rare event cells such as those resulting from a biological warfare agent attack, or for the rapid noninvasive optical assessment of tissue pathology in the detection of cancerous cells).

## Résumé

On documente ici une nouvelle technique faisant une approximation de la diffusion de la lumière laser au moyen de cellules biologiques. Cette technique est basée sur l'approximation d'une équation d'onde scalaire tri dimensionnelle des équations complètes de Maxwell pour le champ électromagnétique. Cette équation d'onde scalaire visant à décrire les modèles de diffusion de la lumière de cellules contenant une structure morphologique (par ex. : organelles variées) est résolue numériquement au moyen d'une méthode spectrale. L'exactitude de cette méthode numérique spectrale est vérifiée en comparant avec des solutions obtenues à partir de la théorie de la perturbation linéaire et de la théorie Mie. La comparaison avec la théorie Mie indique que l'équation d'onde scalaire tri dimensionnelle est une bonne approximation des équations complètes de Maxwell, en ce qui concerne la diffusion de la lumière, tant que ces angles diffusent modérément vers l'avant (angles de diffusion de moins de 35° à peu près). La technique appropriée utilisée ici est capable de prédire correctement les modèles d'intensité diffusés à partir des cellules biologiques à une échelle dynamique comprenant six ordres de magnitude. La nouvelle technique peut être appliquée ici pour calculer la diffusion de la lumière à partir aussi bien d'une cellule biologique individuelle que d'un échantillon contenant un ensemble de ces cellules biologiques. Les modèles d'intensité de diffusion, prédits en utilisant la nouvelle technique, peuvent être appliqués au diagnostic de la taille et de la structure interne des cellules biologiques et devenir un outil d'interprétation précieux en cytométrie de flux (par ex. : dans la détection de cellules rares telles que celles résultant d'une attaque d'agent de guerre biologique ou bien pour l'évaluation optique rapide non effractive de la pathologie des tissus, en ce qui concerne la détection de cellules cancéreuses.

# Executive summary

## Background

A high priority of any biological warfare (BW) agent defence system is the triggering/cueing of the system in the presence of incoming aerosol clouds that may contain the presence of BW agents, followed by the initiation of particulate air sampling required for the subsequent detection and identification of the putative agent in order to warn the user of the presence of a BW agent cloud. In this regard, the problem of the detection of BW agents (e.g., bacteria, viruses) based on some small set of quantifiable properties that can be shown to differ from their immediate background clutter is of great interest. Indeed, this problem was emphasized by Brigadier General Doesberg (Commander, Joint Program Office for Biological Detection, Alexandria, VA) who in his keynote address to a 1996 Edgewood Research, Development, and Engineering Center (ERDEC) scientific conference emphasized that "the major deficiency of our biological detection system is the lack of a reliable triggering/detection device".

The key problem that arises in the detection of a BW agent is to distinguish unambiguously the putative presence of a pathogenic bio-target (BW agent) against the ambient background clutter (which can consist of inorganic matter such as sulfates and nitrates and live non-pathogenic matter such as pollen, fungi and bacteria). Most BW agent detection systems involve drawing an ambient air sample through a laser-illuminated sampling volume where airborne particles scatter light and/or undergo particle fluorescence. Hence, increasing the present understanding of the interaction of laser light with biological cells can potentially improve the ability of current BW agent detection systems to discriminate between a target BW agent and environmental interferents. Understanding the relationship between measured scattered light properties and physiological differences at the cellular level is fundamental to providing a high degree of selectivity for BW agents in current BW detection systems and constitutes the main challenge for the modelling of light scattering from biological cells.

## Principal Results

In this report, we develop a simplified mathematical model for the interaction of laser light with biological cells. In this approach, the full set of Maxwell's field equations is reduced to a wave equation for the electric field. This wave equation is solved numerically using a spectral method. This method provides a computationally efficient numerical scheme that can be used to predict the light scattering intensity pattern from either a single biological cell or a sample containing many biological cells.

The accuracy of the spectral numerical method is verified by comparison with solutions obtained from linear perturbation theory and Mie theory. Comparison with Mie theory shows that the three-dimensional scalar wave equation is a good approximation to the full Maxwell's field equations for light scattering up to moderate forward scattering angles (i.e., for scattering angles less than about $35^\circ$). The approximate technique used here is capable of correctly predicting the scattered intensity patterns from biological cells over a dynamic range spanning six orders of magnitude. The new technique can be applied to calculate the light scattering

either from an individual biological cell and from a sample containing an ensemble of such biological cells. The scattering intensity patterns predicted using the new technique can potentially be applied to diagnose the size and internal structure of biological cells, making it a valuable interpretative tool in flow cytometry (e.g., in the detection of rare event cells such as those resulting from a biological warfare agent attack, or for the rapid noninvasive optical assessment of tissue pathology in the detection of cancerous cells).

## Significance and Future Plans

To improve the performance of BW agent detection systems, it is necessary to understand the relationship between optical and biological properties of BW agents (bacteria, viruses, rickettsiae). A model designed to provide insight into the relationship between the scattering properties of a biological cell and its morphology has been developed in this study. The model can potentially be used to provide deeper insights into the characteristics of laser light scattering from biological cells. In consequence, this fundamental understanding may lead to an improved ability to discriminate biological agents from other harmless biological and non-biological materials present in the ambient environment.

The model developed here provides a capability for interpreting laser light scattering patterns from BW agents, and in particular for assessing cellular morphology from scattering measurements. This will lead to the development of novel analysis methods for flow cytometry which in turn can lead to improvements in BW agent detection. Future work should focus on incorporating a detailed numerical model for prediction of light scattering from biological cells with a new generation of micro-cytometers (viz., flow cytometry undertaken on a microchip) that would allow a more precise interpretation of the data obtained from such a device (and, particularly, in relation to the extraction of morphological parameters from BW agent cells based on scattering measurements).

Shao, Y. and Yee, E. (2004). An Approximate Method for Modelling Laser Light Scattering from Biological Cells. (DRDC Suffield TR 2004-187). Defence R&D Canada – Suffield.

# Sommaire

## Contexte

La grande priorité d'un système de défense contre un agent de guerre biologique (BW) est d'être en mesure de se déclencher ou de signaler l'arrivée de nuages aérosol pouvant contenir des agents BW, puis d'amorcer l'échantillonnage d'air particulier requis pour détecter et identifier ultérieurement l'agent putatif, ceci visant à prévenir l'utilisateur de la présence d'un nuage d'agents BW. À cet égard, il devient très intéressant d'étudier le problème de la détection des agents BW (par ex. : bactéries, virus) en se basant sur un certain petit ensemble de propriétés quantifiables pouvant démontrer qu'un agent diffère du fouillis de son environnement immédiat. Ce problème a été certainement souligné par le brigadier général Doesberg (Commandant du Bureau commun du programme de détection biologique, Alexandria, VA). Dans son discours liminaire à la conférence scientifique de Edgewood Research, Development, and Engineering Center (ERDEC), en 1996, il a souligné que « l'inconvénient majeur de notre système de détection biologique est le manque d'appareil de déclenchement et de détection fiable ». Le problème clé de la détection d'un agent BW est la difficulté de distinguer sans ambiguïté la présence putative d'une cible biologique pathogénique (agent BW) dans le fouillis ambiant de son environnement (pouvant consister en matière non organique telle que les sulfates et les nitrates et de matière vivante non pathogénique telle que le pollen, champignons microscopiques et bactéries). La plupart des systèmes de détection d'agents BW consistent à retirer un échantillon d'air ambiant à l'aide d'un volume d'échantillon illuminé au laser dans lequel les particules aérosol diffusent la lumière et / ou la particule devient fluorescente. Ainsi, une meilleure compréhension de l'interaction entre la lumière laser et les cellules biologiques peut sans doute améliorer la capacité des systèmes actuels de détection d'agents BW à discriminer entre un agent BW cible et ses interférents environnementaux. Il est fondamental de comprendre la relation entre les propriétés de la lumière diffusée mesurée et les différences physiologiques au niveau cellulaire, pour fournir un haut niveau de sélectivité, en ce qui concerne les agents BW dans les systèmes actuels de détection BW et constitue le défi principal dans le domaine de la modélisation de la diffusion de la lumière, à partir de cellules biologiques.

## Résultats principaux

Dans ce rapport, nous développons un modèle mathématique simplifié de l'interaction de la lumière laser avec les cellules biologiques. Cette méthode réduit l'ensemble complet des équations de Maxwell à une équation d'onde pour le champ électrique. L'équation d'onde est résolue numériquement en utilisant une méthode spectrale. Cette méthode fournit un schéma de calcul numérique efficace pouvant être utilisé pour prédire le modèle de l'intensité de la diffusion de la lumière à partir soit d'une seule cellule biologique soit d'un échantillon contenant beaucoup de cellules biologiques.

L'exactitude de cette méthode numérique spectrale est vérifiée en comparant avec des solutions obtenues à partir de la théorie de la perturbation linéaire et de la théorie Mie. La comparaison avec la théorie Mie indique que l'équation d'onde scalaire tri dimensionnelle est une bonne approximation des équations complètes de Maxwell, en ce qui concerne la

diffusion de la lumière, tant que ces angles diffusent modérément vers l'avant (angles de diffusion de moins de 35° à peu près). La technique appropriée utilisée ici est capable de prédire correctement les modèles d'intensité diffusée à partir des cellules biologiques à une échelle dynamique comprenant six ordres de magnitude. La nouvelle technique peut être appliquée ici pour calculer la diffusion de la lumière à partir aussi bien d'une cellule biologique individuelle que d'un échantillon contenant un ensemble de ces cellules biologiques. Les modèles d'intensité de diffusion, prédits en utilisant la nouvelle technique, peuvent être appliqués au diagnostic de la taille et de la structure interne des cellules biologiques, ce qui les rend un outil d'interprétation précieux en cytométrie de flux (par ex. : dans la détection de cellules rares telles que celles résultant d'une attaque d'agent de guerre biologique ou bien encore pour l'évaluation optique rapide non effractive de la pathologie des tissus, en ce qui concerne la détection de cellules cancéreuses.

## La portée des résultats et les plans futurs

Il est nécessaire de comprendre la relation entre les propriétés optiques et biologiques des agents BW (bactérie, virus, rickettsie) pour améliorer la performance des systèmes de détection d'agents BW. Cette étude a développé un modèle conçu pour procurer une connaissance plus approfondie de la relation entre les propriétés de diffusion d'une cellule biologique et sa morphologie. Il est possible que ce modèle soit utilisé pour acquérir une connaissance plus profonde des caractéristiques de la diffusion de la lumière laser à partir de cellules biologiques. Cette connaissance fondamentale peut, par conséquent, aboutir à l'amélioration de la capacité de discriminer les agents biologiques de ceux qui sont moins dangereux et des matériaux non biologiques qui sont présents dans l'environnement ambiant.

Le modèle développé ici donne la capacité d'interpréter les modèles de diffusion de lumière laser à partir d'agents BW. Il permet surtout d'évaluer la morphologie cellulaire à partir des mesures prises pendant la diffusion. Ceci amènera à la mise au point de méthodes d'analyse nouvelles pour la cytométrie de flux qui à son tour peut aboutir à l'amélioration de la détection d'agent BW. Les travaux futurs devraient se concentrer sur l'incorporation de modèles numériques détaillés pour la prédiction de la diffusion de la lumière à partir de cellules biologiques avec une nouvelle génération de micro-cytomètres (viz., cytométrie de flux entreprise sur un microcircuit intégré) qui permettrait une interprétation plus précise des données obtenues à partir d'un tel appareil (et surtout celles en rapport avec l'extraction de paramètres morphologiques à partir de cellules d'agents BW, basée sur les mesures prises durant la diffusion).

Shao, Y. and Yee, E. (2004). An Approximate Method for Modelling Laser Light Scattering from Biological Cells. (DRDC Suffield TR 2004-187). R & D pour la défense Canada – Suffield.

# Table of contents

# List of figures



# List of tables

# Introduction

Lasers have several unique properties, such as monochromaticity, high power, short pulse duration, and coherence, which are particularly useful for biological agent detection and bio-medical applications. Laser medicine is now a rapidly growing research field. The increasing use of laser light for detection of biological warfare (BW) agents and for diagnostic and therapeutic medicine has created a need to understand how laser light interacts with biological cells and propagates through biological tissue. This understanding would result in improved BW agent detection by providing a quantitative interpretation of the signals that are measured, and in bio-medical applications would enable the quantitative analysis of diagnostic measurements leading potentially to an optimal development of therapeutic techniques.

There are five main categories [1, 2, 3] of photo-physical processes in the interaction of laser light with biological tissues. These are non-destructive photo, photo-chemical, photo-thermal, photo-ablative and photo-mechanical interactions. Non-destructive photo interactions mainly concern laser light propagation and scattering in biological tissue, which can be used both for imaging and diagnostics. Photo-chemical interactions involve the absorption of light by specific molecules that are either present in, or added to, a biological tissue sample. Such interactions are the basis for photo-dynamic therapy. Photo-thermal interactions are those where the observed biological effect is due to the deposition of heat in the tissue. Most current laser surgery, such as welding and coagulation, for example, falls into this category. Photo-ablative interactions can occur when photons have sufficient energy to cause the dissociation of biopolymers with a subsequent desorption of the resulting fragments. The threshold power density for this effect to occur is approximately $10^8$ W cm$^{-2}$ for 10 ns laser pulses. Photo-mechanical interactions occur at fluence rates of approximately $10^{10}$ W cm$^{-2}$ for nanosecond laser pulses and $10^{12}$ W cm$^{-2}$ for picosecond pulses. When these pulses illuminate the biological tissue, the dielectric of the tissue experiences a breakdown, and a small volume plasma is produced. The expansion of this plasma creates a shock wave which can mechanically rupture the tissue. These last two types of interaction are complex in terms of their occurrence thresholds and concomitant nonlinear effects.

In this report, we will focus on non-destructive photo interactions of laser light with biological cells, where the optical properties of the biological cell are time invariant and are independent of the probing light field. Optical properties of biological tissue and cells are very important for a wide range of studies ranging from detection/imaging and diagnostic applications, such as cytometry [4], confocal [5] and optical coherence tomography [6] imaging, and fundamental investigations of the sensitivity of a biological cell to light sources [7]. When laser light enters a biological sample, it can be scattered and absorbed. The relative probability of these processes in a given biological cell or tissue sample depends on the laser wavelength [8]. In these applications, laser light from the blue to near-infrared parts of the spectrum is predominantly scattered from local variations in the refractive index between different parts of the biological cell.

Cytometry is the measurement of physical and/or chemical characteristics of biological cells (e.g., bacteria, viruses, etc.). Flow cytometry [9] is a process in which such measurements are

made while the cells or particles are passing through a sampling volume in a fluid stream. During the past 30 years, sophisticated improvements have made flow cytometry a powerful and valuable tool for the quantitative analysis of individual cells or other biological particles. A flow cytometer is an instrument, which can be used to obtain quantitative information based on light scattering or fluorescence emission caused by individual cells (or particles) as they flow rapidly in a fluid stream in front of a light source [4]. The components of a flow cytometer usually include a light source (normally a laser); a sample chamber with a flow cell and a sheath fluid stream; a photodetector or photomultiplier tube (PMT) that collects light and converts it to an electronic signal; a signal processing system that converts the signal from an analog form to a digital format; and a computer to direct operations, store the collected signals, and display data [10]. With the combination of state-of-the-art advances in computer and laser technology, more sophisticated flow cytometers have been developed to obtain objective and precise measurements of multiple characteristic parameters of an individual cell at one time. Such parameters include cell size, cell shape, and cell refractive index. Recently, flow cytometers [e.g., Los Alamos National Laboratory flow cytometer and the Becton Dickenson Flow Cytometer (FACSCaliber)] have been used in bio-detection to determine if particulates collected are biological or inorganic in origin.

Understanding relationships between the measured scattered light properties and physiological characteristics at the cellular level in the biological cell is fundamental to the usefulness of optical diagnostics (e.g., use of flow cytometry for bio-detection) and constitutes the main challenge for the modelling of laser light scattering from cells. The complexity of the scattering media, coupled with comparable spatial scales of inhomogeneity in the dielectric constant and the laser wavelength, limits an analytical approach to the scattering problem. Several numerical procedures have been adoped to deal with the laser light-cell scattering problem from their original physical and engineering applications.

The most complete numerical method is based on the finite-difference time-domain (FDTD) algorithm, which was originally proposed [11] as the method to solve the full set of Maxwell's equations. Since this seminal work, the numerical solution of Maxwell's equations using the FDTD method has been applied to perform electromagnetic simulations in many areas in electrical engineering and related fields such as microwave engineering, remote sensing and subsurface sensing, antenna analysis and design, radar cross-section analysis and design, stealth technology, wireless communication and propagation, and electromagnetic compatibility and electromagnetic interference (EMC/EMI). It is only very recently that some preliminary effort has been expended on the application of electromagnetic simulations to address bioengineering and biotechnology problems. In a recent implementation of the FDTD algorithm to the light-cellular scattering problem [12], [13], the biological cell has been modelled through the inhomogeneous refractive index of its different structures (organelles). The FDTD approach requires large computational resources both in terms of memory and time because the FDTD algorithm solves for the full vector electric and magnetic fields and resolves their evolution on the time scale of a laser light period.

The Monte Carlo (MC) method is a technique first proposed to simulate physical processes using a stochastic model [14] and it has been used to solve a variety of physical problems.

Recently, MC simulations of photon propagation provide a flexible, yet rigorous, approach toward photon propagation in turbid tissues [15]. It should be pointed out that the MC simulations are rigorous, but necessarily statistical in nature and, therefore, require significant computation time to achieve the required precision and resolution. An alternative to the FDTD and MC methods is the discrete dipole approximation [16], [17], in which a particle is divided into subvolumes that are assumed to behave as dipoles.

In summarizing, the FDTD and MC methods are the two mainstream numerical methods for modelling laser light propagation and scattering from biological cells and tissues. The MC method efficiently describes multiple scattering from cells. However, it is not well suited to addressing scattering from a single cell. On the contrary, the FDTD method accurately describes scattering from a single cell, but its application to multiple cell scattering results in computational requirements that increase dramatically with an increase in the size of the computational domain. In view of this, the objectives of this report are: (1) to develop an approximate technique that can be used to predict the scattering intensity patterns from samples consisting of single or multiple biological cell(s); and, (2) to develop, implement, and validate a computer simulation code based on this technique for the modelling and prediction of laser light scattering from biological cells.

The proposed new approximate method for modelling laser light scattering from biological cells is based on a simplified mathematical model of light propagation. The resulting equations of this method are solved numerically using a spectral algorithm. The results of numerical and analytical studies of light scattering from two-dimensional (2-D) and three-dimensional (3-D) cell geometries are presented in this report. In the 2-D cellular scattering studies, the relative change in the angular distribution of scattering intensity due to the internal cell structure, shape, size, and refractive index can be addressed more easily than in three dimensions because the computational burden and memory requirements are smaller. Examples of multiple scattering processes (i.e., dependence of the scattered light characteristics on the number of scatterers and density of cells in the sampling volume) are provided for 2-D cell geometries.

In our approximate simulation approach, the full set of Maxwell's equations is reduced to a wave equation for the electric field. Further approximations include the elimination of high frequency ($\omega_0$) oscillations (carrier frequency of the electromagnetic wave) by enveloping the field amplitude variations that occur on an $\omega_0^{-1}$ time scale, which reduces the order of the time derivative in the wave equation (a detailed explanation of this process is provided later in Section 2). As compared, for example, to numerically solving the full set of Maxwell's equations, we have reduced the number of equations to solve, eliminated the need for temporal resolution on an $\omega_0^{-1}$ time scale, and by applying the spectral method [18] for the numerical solution of the resulting equation have enabled the scattering intensity distribution to be accurately calculated using six grid points per laser wavelength. By reducing the numerical requirements to obtain a solution, we have developed an effective algorithm, which could be applied to studies of scattering from a single biological cell as well as from a sample consisting of ensemble of many biological cells.

# The Computational Model

## Basic Equations of the Approximate Model

The computational model used for the scattering problem considered in this report is based on solving the wave equation for the amplitude of the laser light using the spectral method. This method allows us to model the interaction of laser light with biological cells whose physical size can vary over a wide range of spatial length scales, from sub-wavelength dimensions up to a few orders of magnitude larger than the laser wavelength.

Maxwell's equations in a nonconducting medium take the following form [19] (in Gaussian units):

$$\nabla \cdot \varepsilon \vec{E} = 0, \tag{1}$$

$$\nabla \cdot \vec{B} = 0, \tag{2}$$

$$\nabla \times \vec{E} + \frac{1}{c}\frac{\partial \vec{B}}{\partial t} = 0, \tag{3}$$

$$\nabla \times \vec{B} - \frac{\mu\varepsilon}{c}\frac{\partial \vec{E}}{\partial t} = 0, \tag{4}$$

where $\vec{E}$ and $\vec{B}$ are the electric and magnetic fields, respectively; $c$ is the speed of light in vacuum; and $\mu$ and $\varepsilon$ are the magnetic permeability and the dielectric constant (or, electric permittivity) of the medium, respectively. By taking the curl of Eq. (3) and substituting for $\nabla \times \vec{B}$ from Eq. (4), we deduce the following wave equation for the electric field; namely,

$$\frac{\mu\varepsilon}{c^2}\frac{\partial^2 \vec{E}}{\partial t^2} - \nabla^2 \vec{E} + \nabla(\nabla \cdot \vec{E}) = 0, \tag{5}$$

where we have used the vector identity

$$\nabla \times (\nabla \times \vec{A}) = \nabla(\nabla \cdot \vec{A}) - \nabla^2 \vec{A},$$

and the fact that the operators $\nabla \times \frac{\partial}{\partial t}$ and $\frac{\partial}{\partial t}\nabla \times$ are equivalent (i.e., $\nabla$ and $\frac{\partial}{\partial t}$ commute) as space and time coordinates are independent. Here, $\nabla^2 \equiv \partial^2/\partial x^2 + \partial^2/\partial y^2 + \partial^2/\partial z^2$ denotes the Laplacian in a three-dimensional Cartesian geometry.

For an electromagnetic wave with high frequency $\omega_0$ say, the electric field vector takes the form

$$\vec{\mathrm{E}} = \vec{E}(x,y,z,t)\exp(-i\omega_0 t) + \text{c.c.}, \tag{6}$$

where c.c. denotes the complex conjugate of the first term on the right-hand side of this equation. Here, $\omega_0$ can be interpreted as the carrier frequency of the electromagnetic wave. It is assumed that the amplitude $\vec{E}(x,y,z,t)$ varies on a characteristic time scale that is much larger than the light period $2\pi/\omega_0$. In view of this assumption, enveloping Eq. (5) with respect to time (viz., inserting Eq. (6) into Eq. (5) and ignoring the small-order term $\frac{\partial^2 \vec{E}}{\partial t^2} \ll \omega_0 \frac{\partial \vec{E}}{\partial t}$), reduces the order of the time derivative from two to one. In consequence, one obtains

$$2i\frac{\omega_0}{c^2}\varepsilon\mu\frac{\partial \vec{E}}{\partial t} + \nabla^2 \vec{E} + \frac{\omega_0^2}{c^2}\varepsilon\mu\vec{E} - \nabla(\nabla \cdot \vec{E}) = 0. \tag{7}$$

As a further simplification, we develop a wave equation model for a one-component field (i.e., a scalar wave equation model). For the one-component field case, we consider the scattering of laser light by a biological cell (tissue) in two and three spatial dimensions. A 2-D scalar wave equation can be obtained from Eq. (7) by assuming that the biological cell is inhomogeneous (in electric permittivity) in the *x*-*y* plane only and that the electromagnetic wave is *s*-polarized [viz., $\vec{E} = E(x,y,t)\vec{e}_z$ (where $\vec{e}_z$ is a unit vector normal to the *x*-*y* plane) so that the electric field polarization vector is perpendicular to the plane of inhomogeneity of the biological cell]. For this case, the last term on the left-hand side of Eq. (7) is zero, and one obtains a scalar wave equation for the electric field amplitude of the form $E(x,y,t)$:

$$2i\frac{\omega_0}{c^2}\varepsilon\mu\frac{\partial E}{\partial t} + \nabla_2^2 E + \frac{\omega_0^2}{c^2}\varepsilon\mu E = 0, \tag{8}$$

where $\nabla_2^2 \equiv \partial^2/\partial x^2 + \partial^2/\partial y^2$ is the Laplacian in two spatial dimensions.

The scalar field approximation can be also considered in three spatial dimensions. The form of the wave equation for the 3-D scalar field approximation is similar to that of Eq. (8), except that the Laplacian $\nabla^2$ has three spatial components. For the case of three spatial dimensions, the last term on the left hand side of Eq. (7) may not be negligible. The validity of such an approximation will be tested by comparing simulation results with exact analytical solutions (Mie theory) for scattering from a homogeneous spherical dielectric.

For a biological cell, we assume $\mu = 1$ (non-magnetic), and that the dielectric constant can be represented as a sum of two terms:

$$\varepsilon = \varepsilon_0 + \Delta\varepsilon(x,y,z). \tag{9}$$

Here $\varepsilon_0$ is the dielectric constant of the background fluid (fluid surrounding the biological cell) that is considered homogeneous, and $(\varepsilon_0 + \Delta\varepsilon(x,y,z))$ is the dielectric constant of a cell that consists of cytoplasm, nucleus, and other internal structures and organelles. We note that in Eq. (9) that $\varepsilon$ is real since only light scattering (and, not absorption) is considered. Furthermore, measurements of the optical properties of *Erwinia herbicola* bacteria [20] have shown that the imaginary part of the complex index of refraction $N \equiv \sqrt{\varepsilon}$ is approximately four orders of magnitude smaller than the real part, implying that the extinction (or, absorption) of light in the biological cell is negligible relative to the light scattering. Hence, an arbitrary cell model can be constructed by simply assigning real dielectric constant (or, real electric permittivity) values to each cell component. For the cells considered in this report, the perturbations $\triangle\varepsilon$ are assumed to be small (viz., $|\triangle\varepsilon| \ll \varepsilon_0$).

It is readily seen that the first term on the left-hand side of Eq. (8) accounts for time variations of the electric field amplitude. In the case of interest to us, the biological cell properties are considered to be stationary. Non-stationarity can only play a role during the propagation of the electromagnetic wave front through the biological cell. Hence, $\varepsilon$ can be replaced by $\varepsilon_0$ in the time derivative term in Eq. (8), allowing us to rewrite this equation as (for 2-D and 3-D cell geometries)

$$2i\frac{\omega_0}{c^2}\varepsilon_0\frac{\partial E}{\partial t} + \nabla^2 E + \frac{\omega_0^2}{c^2}\varepsilon_0 E = -\frac{\omega_0^2}{c^2} f(t)\triangle\varepsilon E. \tag{10}$$

The time function $f(t)$ is introduced on the right-hand side of Eq. (10) to model an adiabatic "turn on" of the perturbations with the property that $f(t) = 0$ at $t = 0$ and $f(t) \to 1$ as $t \to \infty$. Fig. 1 shows the time function $f(t)$ that was used for the simulations in this report. This time function $f(t)$ allows one to define an easy problem for which we know the solution (e.g., when $f(t) = 0$ at $t = 0$ corresponding to the case of an electromagnetic wave propagating through a homogeneous medium with no scatterer), and a "path" between this easy problem and the hard problem that we actually wish to solve (viz., electromagnetic scattering from the biological cell which is fully "turned on" in the simulation when $f(t) \to 1$ for large $t$). Hence, the solution to the easy problem is gradually transformed to the solution of the hard problem by tracing this path (which is defined by $f(t)$ increasing monotonically from 0 at $t = 0$ to 1 at large $t$). Though the unit of $t$ is arbitrary, for the simulations conducted in this report we will normalize the time steps so that $t$ is measured in units of picoseconds (see details in the next section).

The left-hand side of Eq. (10) accounts for the field propagation in a homogeneous medium, and the interaction with inhomogeneous perturbations (biological cell) is described by the right-hand side. There are no restrictions in our model on the scale length of spatial variations in $\triangle\varepsilon$. However, inhomogeneities in the scattering medium on a scale length much smaller than the laser wavelength cannot be properly resolved in the scattered light intensity pattern. Therefore, we assume that the characteristic length scale of the spatial inhomogeneity for the perturbation $\triangle\varepsilon$ is larger than the laser wavelength $\lambda_m = c/(\omega_0\sqrt{\varepsilon_0})$ in the background (or, surrounding) medium. Inhomogeneities on a scale length smaller than the wavelength $\lambda_m$ (for example, the interface between the cell and the surrounding fluid, or cell wall) are treated as sharp boundaries in our method. This approach is consistent with the fact that light scattering off an interface much narrower than the wavelength is similar to scattering off a sharp boundary.

## Application of Spectral Method

The wave equation [Eq. (10)] is solved in a three-dimensional domain defined as follows: $0 \le x \le L_x$, $-L_y/2 \le y \le L_y/2$ and $-L_z/2 \le z \le L_z/2$ (see Fig. 2). The incident electromagnetic wave is assumed to be propagating in the $x$-direction. Eq. (10) will be solved using the spectral method [18]. In this method, the electric field amplitude $E$ is expanded as a Fourier series in the transverse ($y$ and $z$) directions as follows:

$$E = \sum_m \sum_{m'} E_{mm'}(x,t) \exp\left(imk_y y + im'k_z z\right), \tag{11}$$

where $k_y = 2\pi/L_y$ and $k_z = 2\pi/L_z$ are the wavenumbers in the $y$- and $z$-directions, respectively. We now introduce the following dimensionless variables:

$$\begin{aligned} T &\equiv \beta\omega_0 t/\varepsilon_0, \\ X &\equiv kx, \\ Y &\equiv ky, \\ Z &\equiv kz, \end{aligned} \tag{12}$$

where $k = 2\pi N/\lambda_0$, with $\lambda_0 = c/\omega_0$ being the laser wavelength in vacuum and $N \equiv \sqrt{\varepsilon_0}$ being the background medium refractive index in the simulation region; and, $\beta$ is a dimensionless

parameter which is used to renormalize the time $T$ to some convenient unit (picoseconds, for example). Using these non-dimensional spatial and temporal variables and the spectral form for the electric field amplitude $E$ exhibited in Eq. (11), Eq. (10) can be re-cast in the following form:

$$\left(2i\beta\frac{\partial}{\partial T}+\frac{\partial^2}{\partial X^2}+K^2_{Xmm'}\right)E_{mm'}=NL(E_{mm'},T), \tag{13}$$

where

$$\begin{aligned} NL(E_{mm'},T) &\equiv -\Delta\varepsilon f(t)E_{mm'}, \\ K^2_{Xmm'} &\equiv \varepsilon_0-(mk_y/k)^2-(m'k_z/k)^2. \end{aligned} \tag{14}$$

The variation of the electric field amplitude $E$ in the longitudinal ($x$) direction is approximated using Chebyshev polynomials $T_n(x)$ of the first kind, which constitute an orthogonal family on the interval $-1\le x\le 1$ with a weight function $1/\sqrt{1-x^2}$. To facilitate this approximation, the extent of the simulation region in the direction of laser light propagation $[0,L_x]$ is mapped into the interval $[-1,1]$. Now, $E_{mm'}(X,T)$ in Eq. (13) is approximated as

$$E_{mm'}(X,T)=\sum_{k=1}^{N_x+1}a_k(T)T_{k-1}(X). \tag{15}$$

The use of Chebyshev polynomials evaluated at collocation (grid) points $X_j$ given by $X_j=-\cos((j-1)\pi/N_x)$, where $j=1,2,\ldots,N_x+1$ and $N_x$ is the total number of points in the $x$-direction allows a fast Fourier transform (FFT) to be used to evaluate $a_k(T)$ in $O((N_x+1)\log(N_x+1))$ operations. Finally, Chebyshev polynomials permit accurate determination of the spatial derivative $\partial^2 E_{mm'}/\partial X^2$ in Eq. (13).

The spectral method used here is more accurate per nodal unknown than any local method (e.g., finite difference, finite volume, or finite element method). For problems with sufficiently smooth solutions and benign (e.g., periodic) boundary conditions, the spectral method results in a considerable computational efficiency.

## Time-stepping Procedure

We use the implicit midpoint rule [21] for the time-stepping of Eq. (13). The implicit midpoint method solves a differential equation of the following form

$$\dot{u}=p(u)u,$$

where $p(u)$ is a given function of the quantity $u$. For a step in time $u^n\to u^{n+1}$, $t_n\to t_{n+1}=t_n+\tau$, where $\tau$ is the time-step size and $u^n$ is the quantity $u$ at $t=t_n$, the implicit midpoint rule reads

$$u^{n+1}=u^n+\tau p(\tilde{u})\tilde{u}, \tag{16}$$

where $\tilde{u} = (u^{n+1} + u^n)/2$ is the midpoint value of $u$. A solution $u^n$ of Eq. (16) is bounded as $n \to \infty$ [22].

Now, it is convenient to rewrite Eq. (13) as

$$\frac{\partial E_{mm'}}{\partial T} = \frac{i}{2\beta}\left(\frac{\partial^2}{\partial X^2} + K_{Xmm'}^2 - \frac{NL(E_{mm'}, T)}{E_{mm'}}\right) E_{mm'}. \tag{17}$$

In order to advance Eq. (17) one time-step, the forward Euler scheme is used to provide a provisional estimate $E_{mm'}^{*(n+1)}$ for $E_{mm'}^{n+1}$ as

$$E_{mm'}^{*(n+1)} = E_{mm'}^n + \tau \left.\frac{dE_{mm'}}{dt}\right|_n, \tag{18}$$

which can be used with $E_{mm'}^n$ to obtain an estimate for the midpoint value $\tilde{E}_{mm'}^n \approx \frac{1}{2}\left(E_{mm'}^n + E_{mm'}^{*(n+1)}\right)$:

$$\tilde{E}_{mm'}^n \approx E_{mm'}^n + \frac{i\tau}{4\beta}\left[\frac{\partial^2 E_{mm'}^n}{\partial X^2} + K_{Xmm'}^2 E_{mm'}^n - NL(E_{mm'}^n, T^n)\right], \tag{19}$$

where Eq. (17) has been used to estimate $\partial E_{mm'}/\partial T\big|_n$. From the implicit midpoint rule [cf. Eq. (16)], we get

$$E_{mm'}^{n+1} = E_{mm'}^n + \frac{i\tau}{2\beta}\left[\frac{\partial^2}{\partial X^2} + K_{Xmm'}^2 - \frac{NL(\tilde{E}_{mm'}, T^n)}{\tilde{E}_{mm'}}\right] \tilde{E}_{mm'}. \tag{20}$$

Substituting Eq. (19) into Eq. (20), assuming that $NL(\tilde{E}_{mm'}, T^n) = NL(E_{mm'}^n, T^n)$, and re-arranging the resulting equation we get

$$E_{mm'}^{n+1} = \tilde{E}_{mm'}^n + \frac{i\tau}{4\beta}\left[\frac{\partial^2}{\partial X^2} + K_{Xmm'}^2\right] E_{mm'}^{n+1} - \frac{i\tau}{4\beta} NL(\tilde{E}_{mm'}, T^n), \tag{21}$$

which can be rewritten as follows

$$\left(\frac{\partial^2}{\partial X^2} - \lambda\right) E_{mm'}^{n+1} = \frac{i4\beta}{\tau}\tilde{E}_{mm'} + NL(\tilde{E}_{mm'}, T^n), \tag{22}$$

where $\lambda \equiv -K_{Xmm'}^2 - i4\beta/\tau$. The length of the simulation region in the direction of light propagation is mapped into interval $[-1, 1]$ and, therefore, Eq. (22) is a Dirichlet problem for a second-order elliptic operator in the interval $[-1, 1]$, which we may solve efficiently using the Tau method [18].

## Boundary Conditions

Among the issues facing the implementation of the numerical algorithms for simulation of electromagnetic fields in complex environments is the proper truncation of the computational domain. In our situation, the problem to be simulated corresponds to an open-region problem, and the numerical implementation requires a proper treatment of the grid boundaries. Due to

the properties of the Fourier transform, the imposed boundary conditions are implicitly periodic in the transverse ($Y$ and $Z$) directions. The boundary conditions in $X$-direction correspond to transparent boundaries at $X = X_l = 0$ (left side domain boundary) and $X = X_r = k_0 L_x$ (right side domain boundary) for both the incident and scattered waves [23]:

$$\begin{aligned}
\left.\frac{\partial E_{mm'}}{\partial X}\right|_{X_l} &= iK_{Xmm'}\left(2E^{(0)}_{mm'}(T) - E_{mm'}(X_l,T) + \right. \\
&\qquad \left. \frac{i\beta}{K^2_{Xmm'}}\frac{\partial}{\partial T}\left[E^{(0)}_{mm'}(T) - E_{mm'}(X_l,T)\right]\right), \\
\left.\frac{\partial E_{mm'}}{\partial X}\right|_{X_r} &= iK_{Xmm'}\left(1 + \frac{i\beta}{K^2_{Xmm'}}\frac{\partial}{\partial T}\right)E_{mm'}(X_r,T),
\end{aligned} \tag{23}$$

where $E^{(0)}_{mm'}(T)$ is the Fourier component of the incident electric field amplitude. The transparent boundary conditions imposed here in the longitudinal direction ensure that spurious reflections from the grid boundaries at $X_l$ and $X_r$ are small enough so that the solution is not contaminated.

## The Shape of the Incident Beam

Two kinds of incident beam shapes are used in our simulations. Firstly, the simplest case is that of an incident plane wave. Secondly, we consider the Gaussian beam [24]

$$\begin{aligned}
E_0(x=0,y,z,t) &= E_0(t)\frac{\sigma}{W(x)}\exp\left[-\frac{y^2+z^2}{2W^2(x)}\right] \\
&\qquad \times \exp\left[-jkx - jk\frac{y^2+z^2}{2R^2(x)} + j\zeta(x)\right],
\end{aligned} \tag{24}$$

where $W(x)$ and $R(x)$ are the beam radius and the wavefront radius, respectively, which take the following forms:

$$W(x) = \sigma\left[1 + \left(\frac{x}{L_R}\right)^2\right]^{1/2}, \tag{25}$$

$$R(x) = x\left[1 + \left(\frac{L_R}{x}\right)^2\right], \tag{26}$$

$$\zeta(x) = \arctan\frac{x}{L_R}, \tag{27}$$

where $\sigma$ is the minimum radius of the beam at the best focus position and $L_R$ is the Rayleigh length, which is the distance from the best focus position to where the beam radius increases by a factor of 2. The minimum radius of the beam is related to the Rayleigh length by

$$\sigma = \left(\frac{\lambda L_R}{2\pi}\right)^{1/2}, \tag{28}$$

where $\lambda$ is the wavelength. The number $f$ is defined to characterize the minimum radius of the beam $\sigma = f\lambda$ at the best focus position and the $f$-number is also related to the Rayleigh length as $L_R = 2\pi f^2\lambda$. The Gaussian profile given in Eq. (24) is a reasonable realization of an actual incident laser beam as it might be found in an experimental setup, while the plane wave is a idealized profile for verifying the correctness of the simulation code, as it allows for a direct comparison with analytical solutions (e.g., Mie theory).

## Far-field Calculation

An appropriate presentation of numerical data is very important for the comparison with experimental results and theoretical models. Typical experimental observations usually only measure the characteristics of the laser light well outside the interaction region (the region where the laser light interacts with the scatterer such as a biological cell). Therefore, the laser field profile far from the scattering object (so-called far-field region) should be calculated from the field distribution in the interaction region (so-called near-field region) which can be obtained through our numerical simulations. Using the near-field data obtained from our model simulations, this near-to-far-field transformation efficiently and accurately calculates the far-field scattering response of an illuminated bio-target (biological cell) without the need to extend the simulation domain to the far field to obtain the far-field data.

An asymptotic expression for the electric field of the scattered light at a far-field point $P$ (see Fig. 2) is given by [25]:

$$\begin{aligned} E(P,t) &= \frac{1}{2i}\oint_S dS\cdot\left[E_s(x,y,z,t)\nabla_n\left(\frac{1}{2\pi k\rho(x,y,z)}\exp\left(ik\rho(x,y,z)-i\pi/4\right)\right)\right. \\ &\left.-\frac{1}{2\pi k\rho(x,y,z)}\exp\left(ik\rho(x,y,z)-i\pi/4\right)\nabla_n E_s(x,y,z,t)\right], \end{aligned} \tag{29}$$

where $E_s$ is the electric field at the emitting surface $S$, $E(P,t)$ is the electric field at a far-field point $P$, $\nabla_n$ denotes the derivative along the outwardly-directed normal vector to the emitting surface, and $\vec{\rho}$ is the vector from the point at the emitting surface with coordinates $(x,y,z)$ to the far-field point with coordinates $(x_0,y_0,z_0)$. Furthermore, let $\vec{\rho_0}$ be the postion vector from the origin of the coordinate system to the far field point [viz., $\vec{\rho_0} = (x_0,y_0,z_0)$]. In order to evaluate the surface integral of Eq. (29), we use a Cartesian geometry and let

$$u \equiv \left(1/2\pi k\rho(x,y,z)\right)\exp\left(ik\rho(x,y,z)-i\pi/4\right).$$

Then the surface integral of Eq. (29) takes the form

$$E(P,t) = \frac{1}{2i}\oint_S dS\cdot(E\nabla_n u - u\nabla_n E). \tag{30}$$

From Fig. 2, one can see that the planes $ABCD$ and $EFGH$ coincide with the inlet $(x=0)$ and outlet $(x=L_x)$ boundaries. For forward scattering calculations, we consider only the

contributions due to plane $EFGH$, while for backward scattering calculations, we consider only the contributions due to plane $ABCD$. Hence, the integral of Eq. (30) reduces to

$$E(P,t) = \frac{1}{2i}\int\int dydz\left(E\frac{\partial u}{\partial x} - u\frac{\partial E}{\partial x}\right). \tag{31}$$

The above result can be expressed in a somewhat more informative form if we rewrite $\vec{\rho}$ in terms of spherical coordinates $(\rho,\theta,\phi)$, where $\rho \equiv \left|\vec{\rho}\right|$. Also, we let $\rho_0 \equiv \left|\vec{\rho_0}\right|$ denote the distance from the origin of the coordinate system to the far field point. Using the following mathematical relationships

$$\begin{aligned}
\partial\rho/\partial x &= -x/\rho = -\cos\theta, \\
\partial u/\partial x &= (\partial u/\partial\rho)(\partial\rho/\partial x) = -\cos\theta(\partial u/\partial\rho), \\
\rho &\simeq \rho_0 - x\cos\theta - y\sin\theta\cos\phi - z\sin\theta\sin\phi, \\
\lim_{\rho\to\infty} u &= \frac{1}{2\pi k\rho_0}\exp(ik\rho_0 - ikx\cos\theta - iky\sin\theta\cos\phi \\
&\quad -ikz\sin\theta\sin\phi - i\pi/4), \\
\lim_{\rho\to\infty}\frac{\partial u}{\partial\rho} &= \frac{ik}{2\pi k\rho_0}\exp(ik\rho_0 - ikx\cos\theta - iky\sin\theta\cos\phi \\
&\quad -ikz\sin\theta\sin\phi - i\pi/4),
\end{aligned} \tag{32}$$

we have

$$\begin{aligned}
E(P,t) &= \frac{1}{2i}\frac{1}{2\pi k\rho_0}\int\int dydz\left[-ikE\cos\theta - \frac{\partial E}{\partial x}\right] \\
&\quad \times\exp\left(-ikx\cos\theta - iky\sin\theta\cos\phi - ikz\sin\theta\sin\phi\right).
\end{aligned} \tag{33}$$

By introducing $k_x = k\cos\theta$, $k_y = k\sin\theta\cos\phi$, $k_z = k\sin\theta\sin\phi$, and taking into account that, in the case of forward scattering, $E \sim \exp(ik_x x)$, one obtains from Eq. (33) that

$$E(P,t) = \frac{\exp(ik\rho + i\pi/4)}{4\pi k\rho_0}\left[-2ik_x\exp(-ik_x x)\right]E(L_x,k_y,k_z). \tag{34}$$

Similarly, in the case of backward scattering, we have

$$E(P,t) = \frac{\exp(ik\rho + i\pi/4)}{4\pi k\rho_0}\left[2ik_x\exp(-ik_x x)\right]E(0,k_y,k_z). \tag{35}$$

Eq. (34) for $E(P,t)$ has been used in our numerical simulations to calculate the forward scattered light intensity in the far-field region. The forward emitted power at a far-field point is then given by

$$Q = \frac{c}{8\pi}\rho_0^2|E(P,t)|^2 = \frac{c}{128\pi^3k^2}\left|ik_xE(L_x,k_y,k_z)\right|^2. \tag{36}$$

# Code Implementation and Verification

In the previous section, we presented the theoretical (albeit approximate) model equations upon which our numerical simulations are based. More specifically, we derived an approximate scalar 3-D wave equation from Maxwell's equations, described the numerical algorithm which we will use to solve this equation, and showed how to compute the scattering pattern in the far-field region using a near-field to far-field integral transformation.

For the model equations described in the previous section for both 2-D and 3-D cell geometries, a computer code has been implemented to solve these model equations using the spectral method. Since the code is new, it needs to be verified before being used for any applications. In this section, results for both 2-D and 3-D cell geometries will be presented and verified against predictions obtained from linear perturbation theory and Mie theory, respectively.

## Linear Perturbation Theory Applied to 2-D Scattering

In this subsection, an analytical stationary solution to Eq. (10) is obtained using the linear perturbation method. In the stationary regime, the time derivative term in Eq. (10) is identically zero. Now, consider the scalar wave equation [Eq. (10)] in two spatial dimensions. By assuming small-angle scattering, the field amplitude $E$ can be written as $E = E_a(x,y)\exp(ik_m x)$, where $k_m \equiv 2\pi/\lambda_m = (\omega_0/c)\sqrt{\varepsilon_0}$ is the laser wavenumber in the background medium. The characteristic inhomogeneity length scale of the field amplitude $E_a(x,y)$ in the direction of light propagation ($x$) is assumed to be much larger than the laser wavelength in the background medium, so $\lambda_m \ll |\partial \ln(E_a)/\partial x|^{-1}$. This is precisely the condition that is required for validity of the paraxial approximation. Expanding $E_a = E_0 + \delta E$ , where $E_0$ is the incident light amplitude and $\delta E$ is the scattered light amplitude ($|\delta E| \ll |E_0|$), Eq. (10) to first order in $\delta E$ and $\Delta\varepsilon$ assumes the form

$$2ik_m \frac{\partial \delta E}{\partial x} + \frac{\partial^2 \delta E}{\partial y^2} + \frac{\omega_0^2}{c^2}\Delta\varepsilon E_0 = 0. \tag{37}$$

After performing a Fourier transformation in the transverse ($y$) direction, we obtain the following differential equation for the Fourier component of the electric field $\delta E(x,k_y)$ :

$$2ik_m \frac{d\delta E(x,k_y)}{dx} - k_y^2 \delta E(x,k_y) + \frac{\omega_0^2}{c^2}\Delta\varepsilon(x,k_y)E_0 = 0, \tag{38}$$

where $\Delta\varepsilon(x,k_y)$ is the Fourier transform of the permittivity perturbation $\Delta\varepsilon(x,y)$ in the $y$-direction. The solution to Eq. (38) takes the form of the following integral transform

$$\delta E(x,k_y) = \frac{i\omega_0^2 E_0}{2k_m c^2}\int_0^x dx' \Delta\varepsilon(x',k_y)\exp\left(-\frac{ik_y^2}{2k_m}(x-x')\right). \tag{39}$$

The constant of integration in Eq. (39) is chosen so that the field perturbation $\delta E$ is zero at the boundary $x = 0$.

For simplicity, consider a square perturbation of the dielectric constant $\Delta\varepsilon(x,y)$ equal to $\Delta\varepsilon_0$ in the region $-R_0 \le x - x_0 \le R_0$ and $-R_0 \le y \le R_0$, and zero elsewhere. By using the assumption that the incident light has a very small divergence angle ($E_0(L_x, k_y) \approx 0$ for $k_y \neq 0$), we may combine Eqs. (39) and (36) to obtain the transmitted power per unit angle as

$$Q = \frac{8E_0^2}{\pi^3 L_y^2}\left(\frac{\Delta\varepsilon_0}{\varepsilon_0}\right)^2 \frac{1-k_*^2}{k_*^6}\sin^2\left(\frac{2\pi R_0}{\lambda_m}k_*\right)\sin^2\left(\frac{\pi R_0}{\lambda_m}k_*^2\right), \tag{40}$$

where $k_* \equiv k_y/k_0$.

Similarly, placing a square nucleus measuring $2R_n$ by $2R_n$ and dielectric constant perturbation $\Delta\varepsilon_n$ in the center of a cell with dimensions $2R_0$ by $2R_0$ and dielectric constant $\Delta\varepsilon_0$, the transmitted power per unit angle is

$$\begin{aligned} Q = \frac{8E_0^2}{\pi^3 L_y^2}\left(\frac{\Delta\varepsilon_0}{\varepsilon_0}\right)^2 \frac{1-k_*^2}{k_*^6}\Bigg[&\sin^2\left(\frac{2\pi R_0}{\lambda_m}k_*\right)\sin^2\left(\frac{\pi R_0}{\lambda_m}k_*^2\right) + \\ 2\left(\frac{\Delta\varepsilon_n}{\Delta\varepsilon_0}-1\right)&\sin\left(\frac{2\pi R_0}{\lambda_m}k_*\right)\sin\left(\frac{\pi R_0}{\lambda_m}k_*^2\right)\sin\left(\frac{2\pi R_n}{\lambda_m}k_*\right)\sin\left(\frac{\pi R_n}{\lambda_m}k_*^2\right) + \\ &\left(\frac{\Delta\varepsilon_n}{\Delta\varepsilon_0}-1\right)^2\sin^2\left(\frac{2\pi R_n}{\lambda_m}k_*\right)\sin^2\left(\frac{\pi R_n}{\lambda_m}k_*^2\right)\Bigg]. \end{aligned} \tag{41}$$

As $k_* \to 0$, Eq. (41) takes the form

$$Q = \frac{32\pi E_0^2}{L_y^2}\left(\frac{\Delta\varepsilon_0}{\varepsilon_0}\right)^2\left(\frac{R_0}{\lambda_m}\right)^4\left[1+2\left(\frac{\Delta\varepsilon_n}{\Delta\varepsilon_0}-1\right)\left(\frac{R_n}{R_0}\right)^2+\left(\frac{\Delta\varepsilon_n}{\Delta\varepsilon_0}-1\right)^2\left(\frac{R_n}{R_0}\right)^4\right]. \tag{42}$$

The scattering from these square perturbations can be used to verify the numerical results obtained from our computer code implementing the spectral method. A comparison between our numerical results and the theoretical predictions of Eqs. (40) and (41) is shown in Fig. 3. In these simulations, the dielectric constant of the medium is $\varepsilon_0 = 1.8225$, while the dielectric constant perturbations for the cytoplasm and the nucleus are $\Delta\varepsilon_0 = 0.0544$ and $\Delta\varepsilon_n = 0.1096$, respectively. The accuracy of our numerical method in this case is clearly demonstrated in Fig. 3, where the numerical simulation results show good agreement with the theoretical calculations.

## Scattering from a 3-D Homogeneous Sphere

The diffraction of a plane monochromatic wave by a homogeneous sphere with a zero thickness interface (no coating on sphere) can be calculated within the framework of Mie theory [25, 26]. Mie theory exactly solves Maxwell's equations in three spatial dimensions for all components of the electromagnetic field both inside and outside the sphere. In Mie theory, the electromagnetic fields are expressed in terms of infinite series expansions. These expansions can be significantly simplified when the distance $r$ from the scattering sphere is much larger than the laser wavelength $\lambda_m$ in the medium surrounding the sphere. When the

incident light is linearly polarized, the scattered light intensity $|S|^2$ can be determined from [26]

$$S = \sum_n \frac{2n+1}{n(n+1)} \left[ a_n \tau_n + b_n \pi_n \right] \tag{43}$$

where $\pi_n = -(1/\sin\theta) dP_n/d\theta$, $\tau_n = -d^2 P_n/d\theta^2$, and $P_n$ are the Legendre polynomials of order $n$. The coefficients $a_n$ and $b_n$ are given by

$$\begin{aligned} a_n &= \frac{m\psi_n(mx)\psi_n'(x) - \psi_n(x)\psi_n'(mx)}{m\psi_n(mx)\xi_n'(x) - \xi_n(x)\psi_n'(mx)}, \\ b_n &= \frac{\psi_n(mx)\psi_n'(x) - m\psi_n(x)\psi_n'(mx)}{\psi_n(mx)\xi_n'(x) - m\xi_n(x)\psi_n'(mx)}, \end{aligned} \tag{44}$$

where $\psi_n$ and $\xi_n$ are the Ricatti-Bessel functions, $x = k_m a$, $m = k_s/k_m$, $a$ is the radius of the scattering sphere, and $k_m$ and $k_s$ are the laser wavenumbers outside and inside the scattering sphere, respectively.

Figs. 4 and 5 compare 3-D simulation results and Mie theory predictions for the scattering of a plane wave by a homogeneous sphere in two different cases. The agreement is very good for scattering angles up to about 30 degrees. This good agreement between our numerical simulations and Mie theory is achieved in spite of the fact that the numerical model solves the wave equation in the scalar approximation only, whereas Mie theory solves the full Maxwell's equations (for all six components of the electromagnetic field). We may conclude that the scalar wave equation is an effective approximation to the full Maxwell equations for moderate scattering angles that are of practical importance for applications such as flow cytometry. The scalar wave approximation is valid because in the case of small-angle scattering, the longitudinal component of the electric field $\vec{E}$ and $\nabla \cdot \vec{E}$ are both small, so the last term on the left-hand side of the full wave equation [Eq. (7)] can be neglected. For larger scattering angles, the scalar wave approximation breaks down, since the term with $\nabla \cdot \vec{E}$ becomes comparable in magnitude to the second and third terms on the left-hand side of Eq. (7).

# Applications and Discussion

The previous two sections dealt with the development of an algorithm upon which our simulations are based and the implementation and verification of the computer code. In this section, we present some preliminary two-dimensional and three-dimensional simulation results of laser light scattering from biological cells to demonstrate some of the potential applications.

The biological cell with typical size in the range of 10-30 $\mu$m consists of various organelles immersed in a cytoplasm, all of which are enclosed within a cell wall [27]. The largest organelle in the cell is usually the nucleus, whose size ranges typically between 3 and 10 $\mu$m [28]. Since we intend to model laser light scattering in biological cells, we require values for the index of refraction of each cell component. The cell is defined by assigning electric permittivity values (or, equivalently, refractive index values) to each cell component. The

values listed in Table 1 were taken from the literature, and are used in all simulations in this report.

| Cell component | Refractive index | Reference |
|---|---|---|
| Surrounding medium | 1.35 | [29] |
| Cytoplasm | 1.37 | [30] |
| Nucleus | 1.39 | [30] |
| Mitochondria | 1.42 | [31] |

***Table 1:*** *The values for index of refraction of various cell components which are used in the simulations. The medium surrounding the cell is assumed to be water.*

## Two-Dimensional Simulation Results

Although they cannot describe the "real world", results from simulations in two dimensions are nevertheless useful in obtaining qualitative predictions for the behaviour of certain systems. The 2-D code is computationally more efficient than the 3-D code, and is advantageous in that memory requirements are modest. Nevertheless, it is expected that the 2-D scattering solutions from heterogeneous biological cells will exhibit *qualitatively* similar trends to the more complex 3-D solutions. In the 2-D case, we will focus on plane-wave scattering from both single and multiple biological cells in the sampling volume.

In light scattering from cells, it is important to understand the role of a cell's nucleus on the scattering intensity pattern. To this end, the first set of simulations was designed to demonstrate how the size of the nucleus in a cell contributes to scattering. Three types of biological cell morphologies were chosen for our 2-D simulations: namely, a cell without a nucleus, a cell with a normal-size nucleus of diameter $D_n = 3$ $\mu$m, and a cell with a large nucleus of diameter $D_n = 6$ $\mu$m (for example, it is known that cancerous cells are characterized by a large nuclear-to-cytoplasmic volume ratio [32]). For our simulations, the biological cell diameter in all three cases is taken to be $D_0 = 11$ $\mu$m, which is within the range of typical biological cell sizes cited above (more, specifically, this size is typical for an animal cell, but is generally larger than a bacterial cell). The dielectric constant (or, electric permittivity) $\varepsilon$ is related to the index of refraction $N$ by $\varepsilon = N^2$. Therefore, using the values from Table 1, we know that the dielectric constant of the surrounding medium (water) is $\varepsilon_0 = 1.8225$. Similarly, we find that for the cytoplasm, $\varepsilon = 1.8769$, while for the nucleus $\varepsilon = 1.9321$. The incident laser light is assumed to be a monochromatic plane wave with wavelength $\lambda_0 = 1$ $\mu$m (near infrared region). The dependence of the scattered light intensity on the scattering angle is shown on a linear scale in Fig. 6(a) and on a logarithmic scale in Fig. 6(b). The transmitted component, which is the large peak at 0 degree in Fig. 6(b), is removed by setting the intensity at 0 degree equal to its neighbouring point intensity in Fig. 6(a).

From Fig. 6, it is clear that the dominant feature of the scattering pattern is contributed by the forward (small-angle) scattering. Three different regions can be identified in the scattering pattern in Fig. 6. First, the angular interval from 0 to 0.25 degrees corresponds to the angular

width of the incident light. The large scattering intensity over this range simply represents the signal from the incident light that is not scattered. The second region, which extends from 0.25 to $\theta_0 \approx 4$ degrees, contains the main part of the scattered light intensity from the biological cell. The width of this interval, characterized by the value of $\theta_0$, is determined by the ratio of the typical cell size to the laser wavelength in the surrounding medium. A cell with a large nucleus scatters more light than a cell with a normal nucleus, while a cell with a normal nucleus scatters more light than a cell without a nucleus. This is consistent with the predictions of linear perturbation theory [Eqs. (41) and (42)] and with the FDTD numerical results of [12]. Finally, for angles larger than $\theta_0 \approx 4$ degrees, the scattering amplitude decreases rapidly with increasing scattering angle, so that the large-angle scattering intensity is small in magnitude.

In many realistic situations, the laser light propagates through a medium (sampling volume) with many scattering objects (scatterers). For example, a sampling volume probed by the laser light may contain many biological cells. Therefore, the problem of light scattering by an ensemble of identical scatterers is of fundamental importance. Next, the scattering pattern of a scattering volume containing many scattering objects will be described and compared to the scattering pattern of a single scatterer. In our 2-D simulations, the number of randomly distributed scattering objects in the simulation region was varied from 1 to 90. The scattering objects are assumed to be homogeneous spheres each with a diameter of $D_0 = 7$ $\mu$m and permittivity of $\varepsilon = 1.8769$. The permittivity of the surrounding medium (water) is assumed to be $\varepsilon_0 = 1.8225$. The incident light is taken to be a monochromatic plane wave with a wavelength $\lambda_0 = 1$ $\mu$m.

Fig. 7 illustrates the typical form of the relationship between the scattering intensity and the scattering angle for the case of 10 random scatterers and of a single scatterer in the simulation domain. It is readily seen that the scattering intensity from 10 scatterers does not have the regular pattern of minima and maxima that is observed for laser light scattering from only a single scattering center. Not surprisingly, the scattering intensity, averaged over an angular interval of a few degrees, is several times larger for the 10 scatterer case than for the single scatterer case. The increase in the scattering intensity with an increasing number of scatterers in the sampling volume is observed at both small and large scattering angles. One can conclude from Fig. 7 that the increase in the number of scatterers changes the magnitude of the scattering intensity, but although the broad characteristic angular features of the scattering pattern are roughly unchanged compared to that of a single scatterer it is seen that the random distribution of the multiple scatterers results also in a complex microstructure being superimposed on the general scattering pattern.

The dependence of scattering power and scattering angle on the number of scatterers is illustrated in Figs. 8(top) and (bottom), which combine results corresponding to two different lengths of the simulation region; namely, $L_x = 160$ $\mu$m and $L_x = 320$ $\mu$m. Fig. 8(top) shows the fraction of the scattered power (i.e., the power of light propagating outside the incident beam optics) as a function of the number of scatterers. The scattered power varies from about 4% for a single scatterer to over 90% for 90 scattering centers. From Fig. 8(top), it is evident that the scattered power does not depend on the length of the simulation region (sampling volume), but only on the number of scatterers contained in the sampling volume. The scattered power is

nearly linearly dependent on the number of scatterers in the sampling volume [cf. Fig. 8(top)].

The angular width of the scattered light can be characterized by the average scattering angle $\langle\theta\rangle$, defined as

$$\langle\theta\rangle = \left( \frac{\int \theta^2 Q(\theta)\, d\theta}{\int Q(\theta)\, d\theta} \right)^{1/2}, \tag{45}$$

where $Q$ is the transmitted power per unit angle. Fig. 8(bottom) shows the dependence of the average scattering angle $\langle\theta\rangle$ on the number of scatterers. It is evident from this figure that $\langle\theta\rangle$ changes only slightly (by no more than about 25%) when the number of scatterers changes from 1 to 90. The small dependence of the characteristic scattering angle $\langle\theta\rangle$ on number of scatterers is consistent with the angular spectrum of the scattering intensity that showed an increase in the amount of scattering without essential changes in the angular spectrum [cf. Fig. 7].

It has been demonstrated that the spectral method can be applied to model laser light scattering from scattering volumes that contain a single biological cell or a large number of biological cells. In the case of laser light scattering from a single biological cell, the most significant features of the angular distribution of the scattered light from various cells occur at small angles. Cells containing large nuclei have more scattering power at small angles compared to cells containing normal-sized nuclei. The amplitude of the scattered light decreases even further for cells without a nucleus. In the case of scattering from multiple cells, the simulation results show that the fraction of the scattered power depends on the number of scatterers and not on the size of the simulation region. In fact, the fraction of the scattered power is almost linearly proportional to the number of scatterers. Finally, the scattering pattern from many cells still roughly retains the angular distribution characteristics of single cell forward scattering, but with a high frequency modulation due to interference effects.

## Three-Dimensional Simulation Results

Since the three-dimensional model more closely describes real-world applications, the results from the 3-D simulations are very useful in obtaining quantitative predictions for the behaviour of laser-cell interactions. In consequence, these results have many potential applications not the least of which is to allow one to assess (diagnose) biological cell morphology from light scattering measurements such as those obtained in flow cytometry measurements. The latter application can lead potentially to improved detection performance for BW agents.

In the 3-D case, the incident laser light profile can either take the form of a plane wave or, more realistically, that of a Gaussian beam. In this subsection, the influence of cell size and nucleus size on the scattering intensity are studied. Figs. 9–12 show the angular spectra of light scattered by a concentric spherical cell in 3-D numerical simulations. The angular range shown in Figs. 9–12 is up to 45 degrees away from the direction of incident light propagation. Fig. 9 shows the angular spectra of scattered light for the case when the incident laser light is a monochromatic plane wave with wavelength $\lambda_0 = 1\ \mu$m. The length of the simulation region is $40\lambda_0$ in the direction of light propagation ($x$-direction) and $80\lambda_0$ in each of the two transverse directions ($y$- and $z$-directions). In Fig. 9, three types of cells are used in our 3-D simulations;

namely, a cell without a nucleus, a cell with a normal-sized nucleus (the diameter of the nucleus $D_n = 3$ $\mu$m), and a cell with a large nucleus (the diameter of the nucleus $D_n = 6$ $\mu$m). The cell diameter in all cases is $D_0 = 11$ $\mu$m. The refractive index of the surrounding medium is assumed to be $N_0 = \sqrt{\varepsilon_0} = 1.35$. The heterogeneous cell is modelled as a concentric spherical geometry (cytoplasm plus nucleus) with refractive indices of $N = 1.37$ and 1.39 for the cytoplasm and nucleus, respectively. A spherical nucleus is located at the center of the spherical cell.

Fig. 10 shows the angular scattering spectra for cells without a nucleus, but with different diameters (sizes); namely, for $D_0 = 11$ $\mu$m, $D_0 = 7$ $\mu$m, and $D_0 = 5$ $\mu$m. The scattering intensity patterns in Figs. 9 and 10 have sharp maxima at zero angle, corresponding to the unscattered (transmitted) light. In our simulations with a plane wave, only a small fraction of light is scattered because the cell volume occupies only a small fraction of the simulation region. Figs. 9 and 10 clearly show that the scattered light spectra have a characteristic width of a few degrees and that this width is consistent with the cell size; viz., the smaller the cell size, the larger the angular width of the main lobe of the scattered intensity pattern. In fact, the first minimum in the scattering pattern is approximately determined by the ratio of the incident laser wavelength and the diameter of the cell. For example, the three cases of cell diameter shown in Fig. 10 have minima at $(1/11) \times 57.3^\circ \approx 5.2^\circ$, $(1/7) \times 57.3^\circ \approx 8.2^\circ$, and $(1/5) \times 57.3^\circ \approx 11.4^\circ$, respectively, for biological cells with diameters of 11, 7, and 5 $\mu$m. This observation is consistent (approximately or better) with diffraction theory (e.g., the intensity distribution of diffraction from a spherical particle of diameter $d$ will have have its first minimum roughly at angle $\theta \approx \lambda/d$, where $\lambda$ is the wavelength of the incident light beam which is consistent with the results shown in Fig. 10).

Figs. 11 and 12 show the angular spectra of scattered light in the case when the incident laser light is a Gaussian beam with a wavelength of $\lambda_0 = 1.0$ $\mu$m and optical $f$-numbers of $f/3$ (Fig. 11) and $f/10$ (Fig. 12). The results of Fig. 11 are for scattering from homogeneous and nucleated spherical cells each with a diameter of 11 $\mu$m, whereas those of Fig. 12 are for homogeneous spherical cells of different diameters. By comparing Figs. 11 and 12 with Figs. 9 and 10, it can be seen that in the case of a Gaussian beam, the amount of scattered light is much larger than in the case of a plane wave. This is partially due to a stronger concentration of the total light beam on a cell. The amount of scattered light can provide information about the permittivity of a cell. This information, combined with the information on the cell size from the width of the angular spectrum, allows a characterization of the basic cellular features.

Figs. 11 and 12 also show that the transmitted component of the incident light dominates the angular spectra of the scattered light. In order to analyze properly the scattered light intensity pattern, the transmitted component of incident light must be removed. If the incident laser light impinges directly on a biological cell and a detector is placed in the forward direction to measure the forward scattering light intensity pattern (i.e., the scattering intensity at small scattering angles), then it seems that a straightforward solution to the problem would be to simply insert an small opaque disc in front of the detector to block the transmitted component of the incident light. However, the problem with this simple solution is that diffraction effects arising from the disc edge will distort the scattering intensity pattern in the forward direction.

A much more elegant solution to this problem would be to use a metal clad leaky waveguide to detect the scattered intensity spectrum as described recently in [33]. The basic idea here is to measure the light scattering pattern from a bio-target resulting not from the incident laser light illumination, but rather from an evanescent wave illumination generated as a guided optical wave in a metal clad waveguide device.

# Summary and Conclusions

This report presents some preliminary results from numerical and theoretical studies of the effects of permittivity heterogeneities on light scattering properties from biological cells and, in particular, of how two major parts of the cell contribute to this scattering. The spectral method is applied to solve two- and three-dimensional scalar wave equations that are used to approximate the full set of Maxwell's equations. We have implemented both 2-D and 3-D solvers for these scalar wave equations and applied them to the prediction of the scattered intensity patterns from biological cells containing heterogeneous organelles.

The accuracy of the 2-D scalar solver has been verified by comparison with linear perturbation theory. Furthermore, Mie theory has been applied to verify the 3-D scalar solver for a homogeneous spherical scatterer. A comparison of the scattered intensity for a homogeneous spherical scatterer also demonstrated that the 3-D scalar wave equation provides a good approximation to the full set of Maxwell's equations for light scattering at small to moderate angles (up to about $35^\circ$).

The simulation code can be used to model light scattering from both a single cell or a large number of cells in the sampling volume (simulation region). The spectral method used to solve the scalar wave equations here allows a very high spatial resolution, limited only by the dimensions of the simulation region (box) in the transverse direction. For example, if the laser wavelength $\lambda_0$ is 1.0 $\mu$m and $L_y = L_z = 80\lambda_0$, then the resolution is $\approx 0.53$ degrees, which is comparable to the resolution attainable in experimental measurements using a flow cytometer. The methodology accurately models cell inhomogeneities on spatial scales larger than the laser wavelength, and treats inhomogeneities with a spatial scale much smaller than the laser wavelength as sharp boundaries. The computational requirements for application of a spectral method (using the fast Fourier transform algorithm) to the solution of a scalar wave equation are much lower than those for solution of the full set of Maxwell's equations using a numerical method such a finite-difference time-domain (FDTD) method which would involve discretizing Maxwell's curl equations in space and time to give a set of explicit finite-difference equations that would need to be stepped in time (with the electric and magnetic fields at each grid point in the simulation domain being alternately updated). However, the price paid for this computational efficiency is that the current model only solves a scalar wave equation so all polarization information is lost. Furthermore, the method cannot resolve explicitly structures (e.g., cell membrane) on scales smaller than the probing laser wavelength.

This page intentionally left blank.

# References


1. London, R. A., Glinsky, M. E., Zimmerman, G. B. and Bailey, D. S. (1997). Laser-tissue interaction modeling with LATIS. *J. Appl. Optics*, 36, 9068–9074.

2. Patterson, M. S., Wilson, C. B. and Wyman, D. R. (1991). The propagation of optical radiation in tissue I. *Lasers in Medical Science*, 6, 155–168.

3. Boulnois, J. L. (1986). Photophysical processes in recent medical laser developments: a review. *Lasers in Medical Science*, 1, 47–66.

4. Gilman-Sachs, A. (1994). Flow cytometry. *Anal. Chem.*, 66, 700A–707A.

5. Rajadhyaksha, M., Grossman, M., Esterwitz, D. and Webb, R. (1995). In-vivo confocal scanning laser microscope of human skin: melanin provides strong contrast. *Journal of Investigative Dermatology*, 104, 946–952.

6. Izatt, J., Hee, M., Huang, D. and Swanson, A. (1993). Micron-resolution biomedical imaging with optical coherence tomography. *Opt. Photonics News*, 4, 14.

7. Albrecht-Buehler, G. (1991). Surface extensions of 3T3 cells towards distant infrared sources. *J. Cell. Biol.*, 114, 493–502.

8. Patterson, M. S., Wilson, C. B. and Wyman, D. R. (1991). The propagation of optical radiation in tissue II. *Lasers in Medical Science*, 6, 379–390.

9. Shapiro, H. M. (1988). Practical Flow Cytometry, New York: Alan R. Liss.

10. Lovett, E. J., Schnitzer, B., Keren, D. F. and Flint, A. (1984). Application of flow cytometry to diagnostic pathology. *Lab. Invest.*, 50, 115–140.

11. Yee, K. (1966). Numerical solution of initial boundary value problems involving Maxwell's equations in isotropic media. *IEEE Trans. Antennas Propagation*, 14, 302–307.

12. Dunn, A. and Richards-Kortum, R. (1996). Three dimensional computation of light scattering from cells. *IEEE Journal of Selected Topics in Quantum Electronics*, 2, 898–894.

13. Dunn, A., Smithpeter, C., Welch, A. J. and Richards-Kortum, R. (1997). Finite-difference time-domain simulation of light scattering from single cells. *Journal of Biomedical Optics*, 2, 262–266.

14. Metropolis, N. and Ulam, S. (1949). Monte Carlo Method. *Journal of the American Statistical Association*, 44, 335–341.

15. Welch, A. J. and van Gemert, M. J. C. (1995). Optical-Thermal Response of Laser-Irradiated Tissue, New York: Plenum.

16. Purcell, E. M. and Pennypacker, C. R. (1973). Scattering and Absorption of Light by Nonspherical Dielectric Grains. *Astrophys. J.*, 186, 705.

17. Hoekstra, A. and Sloot, P. (1994). New Computational Technique to Simulate Light Scattering from Arbitrary Particles. *Particle System Characterization*, 11, 189.

18. Canuto, C., Hussaini, M. Y. and Zang, A. T. A. (1988). Spectral Methods in Fluid Dynamics, Berlin Heidelberg: Springer-Verlag.

19. Jackson, J. D. (1974). Classical Electrodynamics, New York: John Wiley and Sons, Inc.

20. Arakawa, E. T., Tuminello, P. S., Khare, B. N. and Milham, M. E. (2003). Optical Properties of *Erwinia herbicola* Bacteria at 0.190–2.50 $\mu$m. *Biopolymers (Biospectroscopy)*, 72, 391–398.

21. Sanz-Serna, J. M. and Manoranjan, V. S. (1983). A method for the integration in time of certain partial differential equations. *J. Comp. Phys.*, 52, 273–289.

22. Sanz-Serna, J. M. and Verwer, J. G. (1986). Conservative and nonconservative schemes for the solution of the nonlinear Schrodinger equation. *IMA Journal of Numerical Analysis*, 6, 25–42.

23. Amin, M. R., Capjack, C. E. and Rozmus, W. (1993). Two dimensional simulations of stimulated Brillouin scattering in laser produced plasmas. *Phys. Rev. Lett.*, 71, 81–84.

24. Saleh, B. E. A. and Teich, M. C. (1991). Fundamentals of Photonics, New York: Wiley.

25. Born, M. and Wolf, E. (1970). Principles of Optics, Oxford: Pergamon.

26. Mie, G. (1908). Beitrage zur Optik Truber Medien speziell kolloidaler Metallosungen. *Ann. d. Physik*, 25, 377–445.

27. Kapit, W., Macey, R. and Meisami, E. (1987). The Physiology Coloring Book, Cambridge: Harper Collins.

28. Ganong, W. (1993). Review of Medical Physiology, Norwalk, Connecticut: Appleton and Lange.

29. Maier, J., Fantini, S. Walker S., Franceschini, M. and Gratton, E. (1994). Possible correlation between blood glucose concentration and the reduced scattering coefficient of tissues in the near infrared. *Opt. Lett.*, 19, 2062–2064.

30. Brunsting, A. and Mullaney, P. (1974). Differential light scattering from spherical mammalian cells. *Biophys. J.*, 14, 439–453.

31. Liu, H., Beauvoit, B. and Kimura, M. (1996). Dependence of tissue optical properties on solute-induced changes in refractive index and osmolarity. *J. Biomed. Opt.*, 1, 200–211.

32. Mourant, J., Bigio, I., Boger, J. and Conn, R. (1995). Spectroscopic diagnosis of bladder cancer with elastic light scattering. *Laser Surg. Med.*, 17, 350–357.

33. Zourob, M., Mohr, S., Brown, B. J. T., Fielden, P. R., McDonnell, M. and Goddard, N. J. (2003). The development of a metal clad leaky waveguide sensor for the detection of particles. *Sensors and Actuators B (Chemical)*, 90, 297–307.

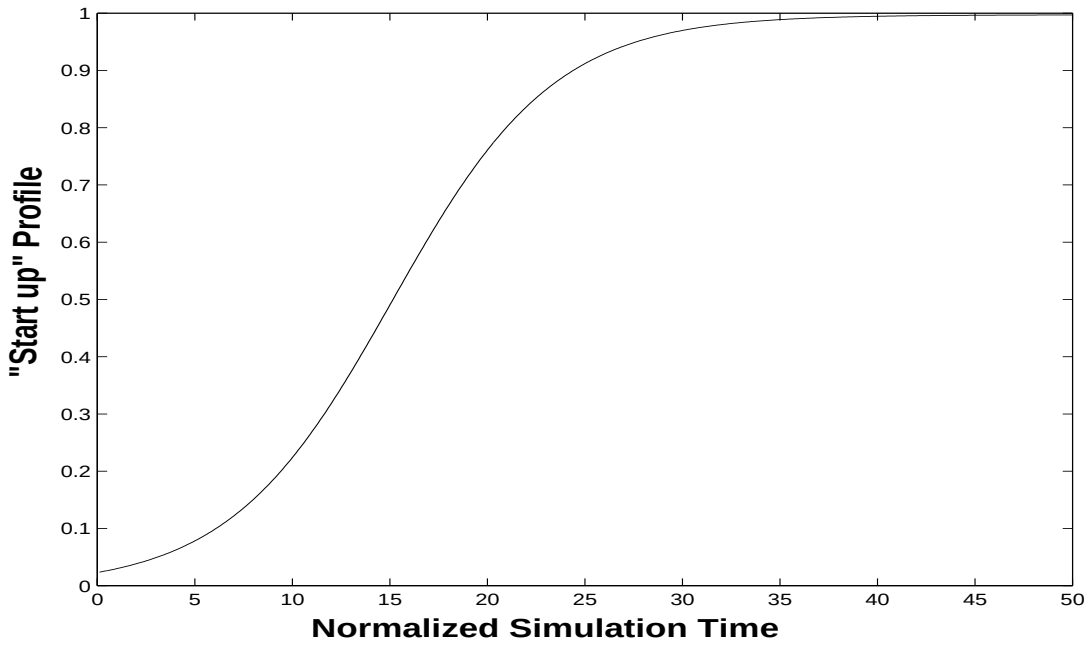


***Figure 1:*** *The profile of time function f(t) which is used to "turn on" the perturbations. Here the simulation time is normalized and a stationary solution is generated in the time interval from 40 to 50 ps.*

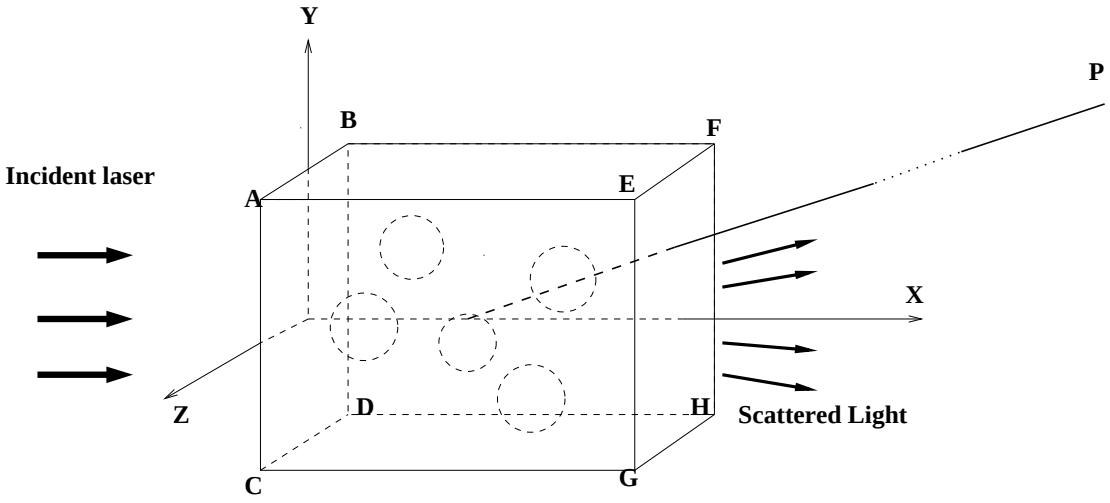


***Figure 2:*** *The geometry of the simulation region.*

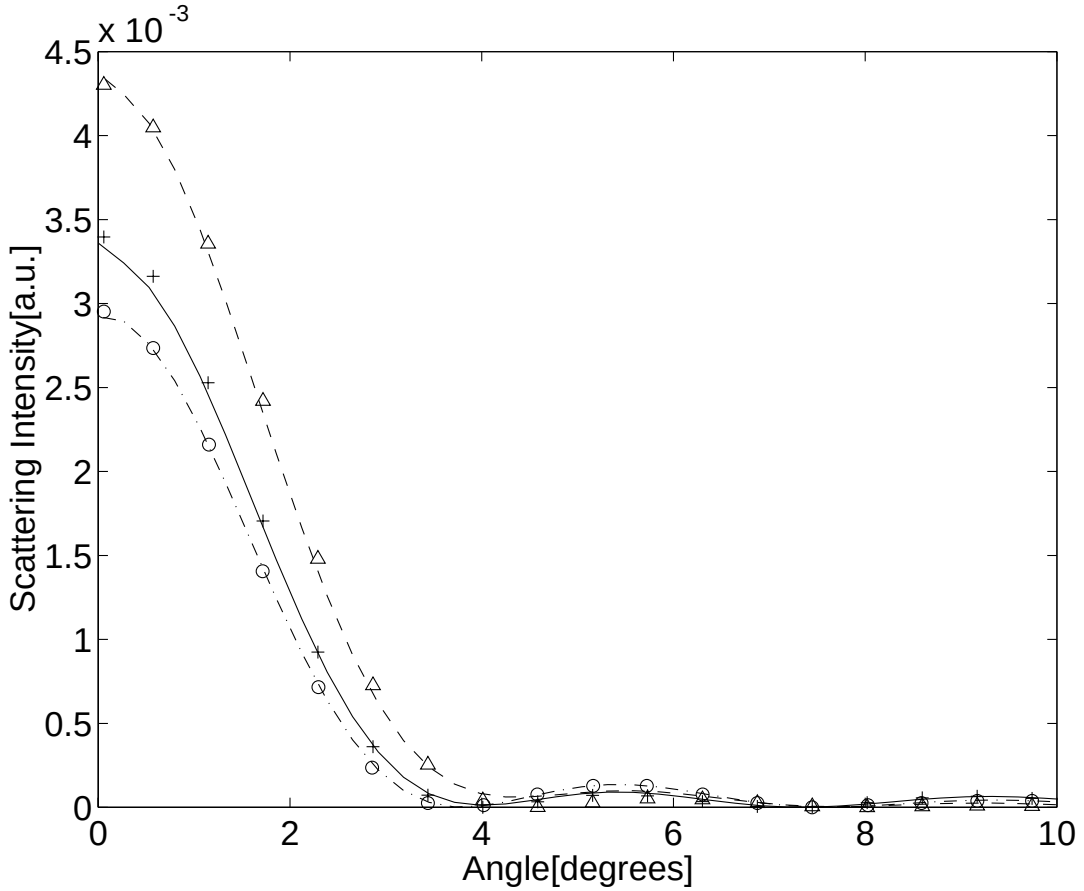


***Figure 3:*** *A comparison of the scattering intensity obtained from both numerical simulations and analytic solutions [Eq. (42)] for three types of square cells: for a cell without a nucleus—the dash-dotted line (simulations) and ∘ (analytical); for a cell with a normal nucleus—the solid line (simulations) and + (analytical); and for a cell with a large nucleus—the dashed line (simulations) and △ (analytical). The diameter of the cell is $D_0 = 11$ μm, the width of the normal nucleus is $D_n = 3$ μm, and the width of the large nucleus is $D_n = 6$ μm. The dielectric constant perturbation for the cytoplasm is $\Delta\varepsilon_0 = 0.0544$, while that for the nucleus is $\Delta\varepsilon_n = 0.1096$.*

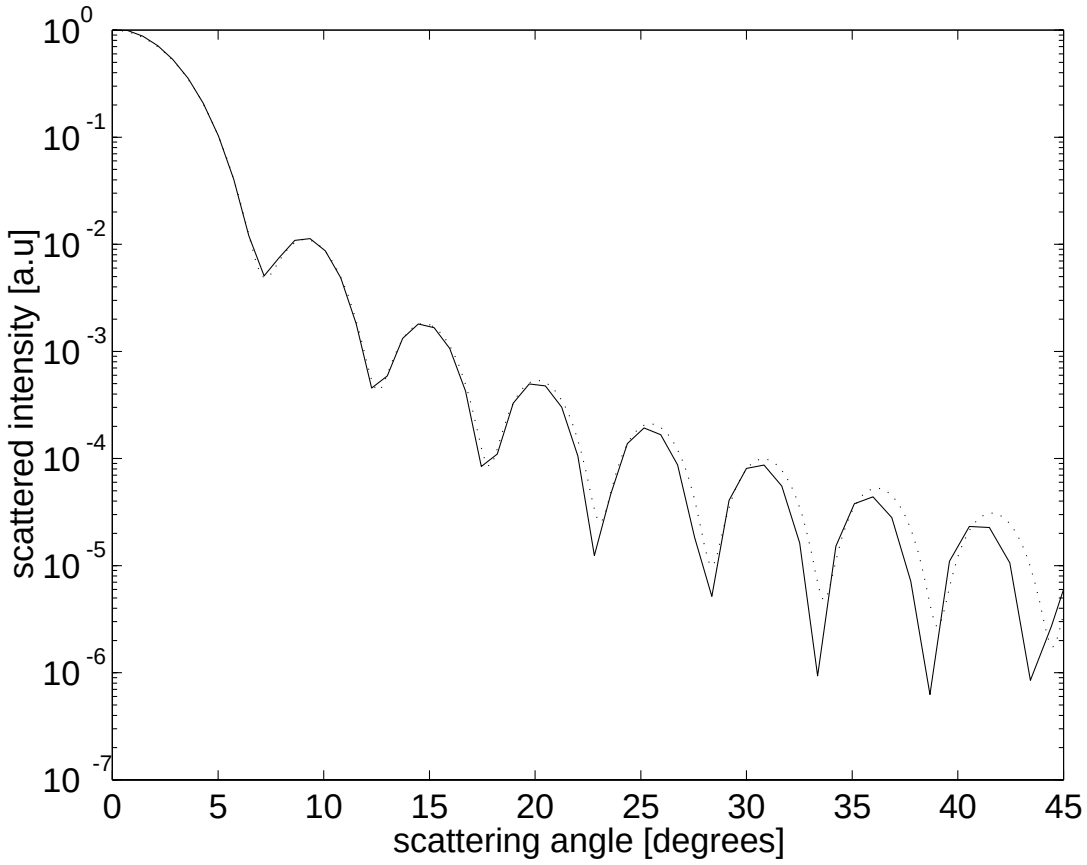


***Figure 4:*** *A comparison of the intensity of scattered light from a homogeneous sphere in three spatial dimensions obtained from simulations (solid line) and from Mie theory (dotted line). The diameter of the sphere is* $D_0 = 11$ *μm. The dielectric constant outside the sphere is* $\varepsilon_0 = 1$ *and inside the sphere is* $\varepsilon = 1.0609$*. In the simulation result, the transmitted component (at* $0^\circ$*) has been removed by setting the intensity here equal to its neighbouring point.*

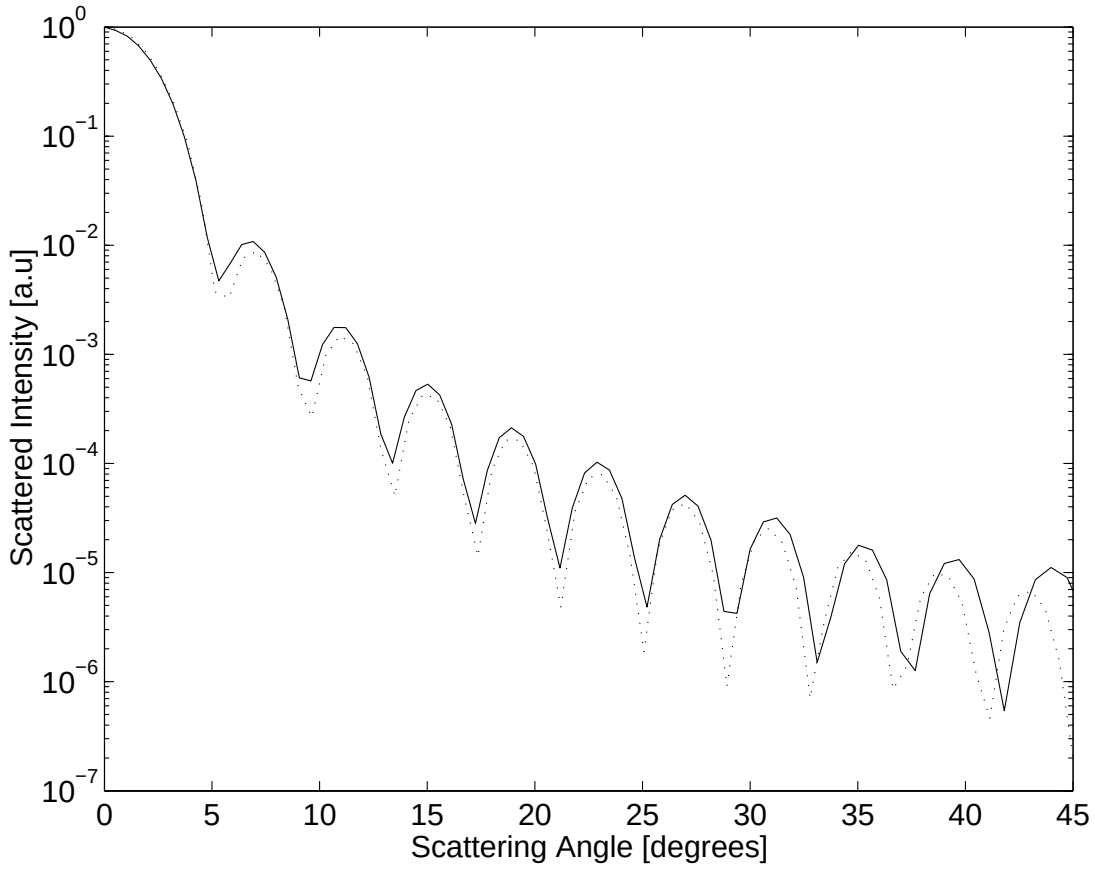


***Figure 5:*** *Another comparison of the intensity of scattered light from a homogeneous sphere in three spatial dimensions obtained from simulations (solid line) and from Mie theory (dotted line). The diameter of the sphere is* $D_0 = 11$ *μm. The dielectric constant outside the sphere is* $\varepsilon_0 = 1.8225$ *and inside the sphere is* $\varepsilon = 1.8769$*. In the simulation result, the transmitted component (at 0°) has been removed by setting the intensity here equal to its neighbouring point.*

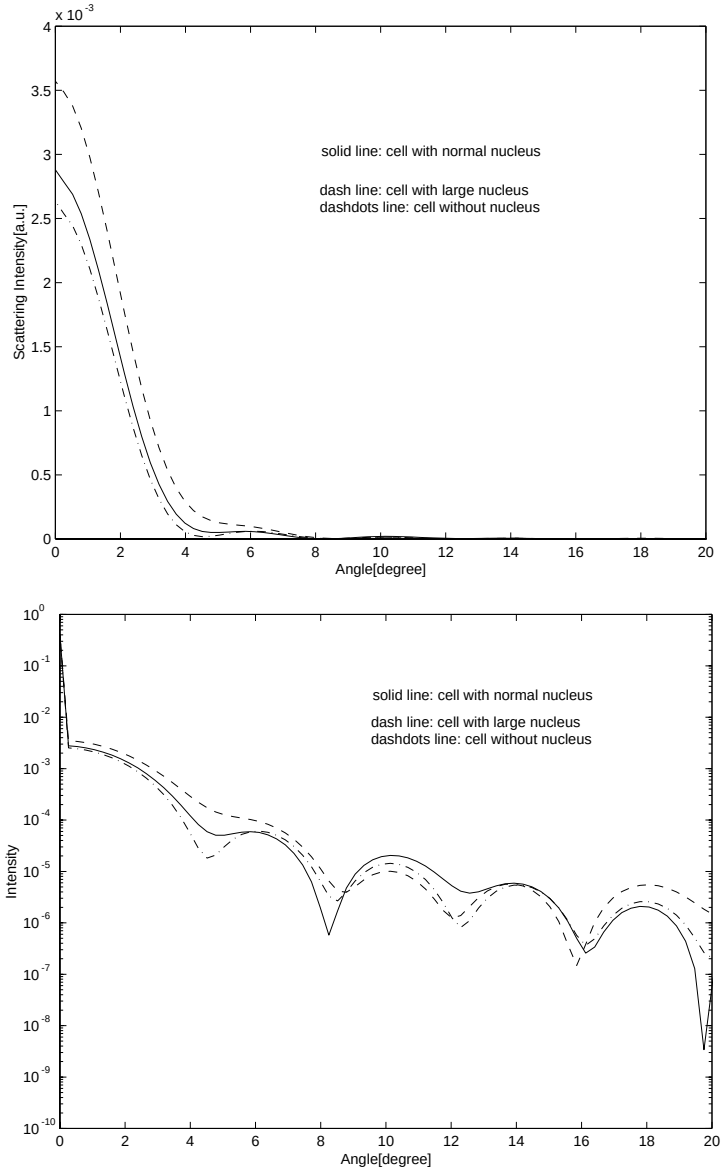


***Figure 6:*** *Scattering intensity from a two-dimensional single cell with diameter $D_0 = 11$ μm on a linear scale (top) and a semi-logarithmic scale (bottom). The dash-dotted line corresponds to a cell without nucleus, the solid line corresponds to a cell with a normal nucleus of diameter $D_n = 3$ μm, and the dashed line corresponds to a cell with a large nucleus of diameter $D_n = 6$ μm. The transmitted component, which is the large peak at 0° (bottom), is removed by setting the intensity here equal to a neighbouring point intensity (top).*

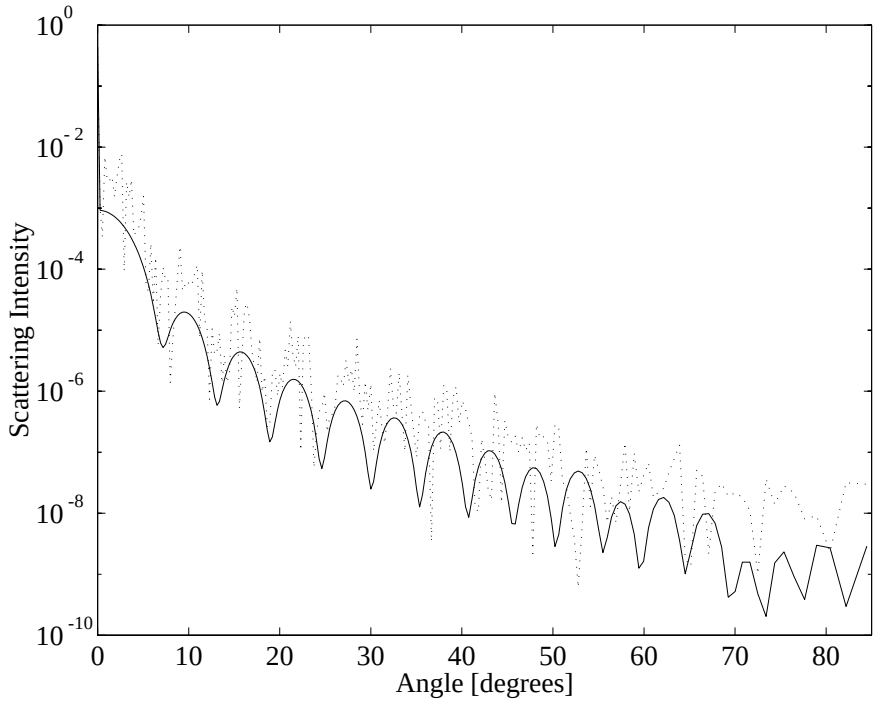


***Figure 7:*** *Scattering intensity as a function of scattering angle for 10 scatterers (dotted line) and for a single scatterer (solid line).*

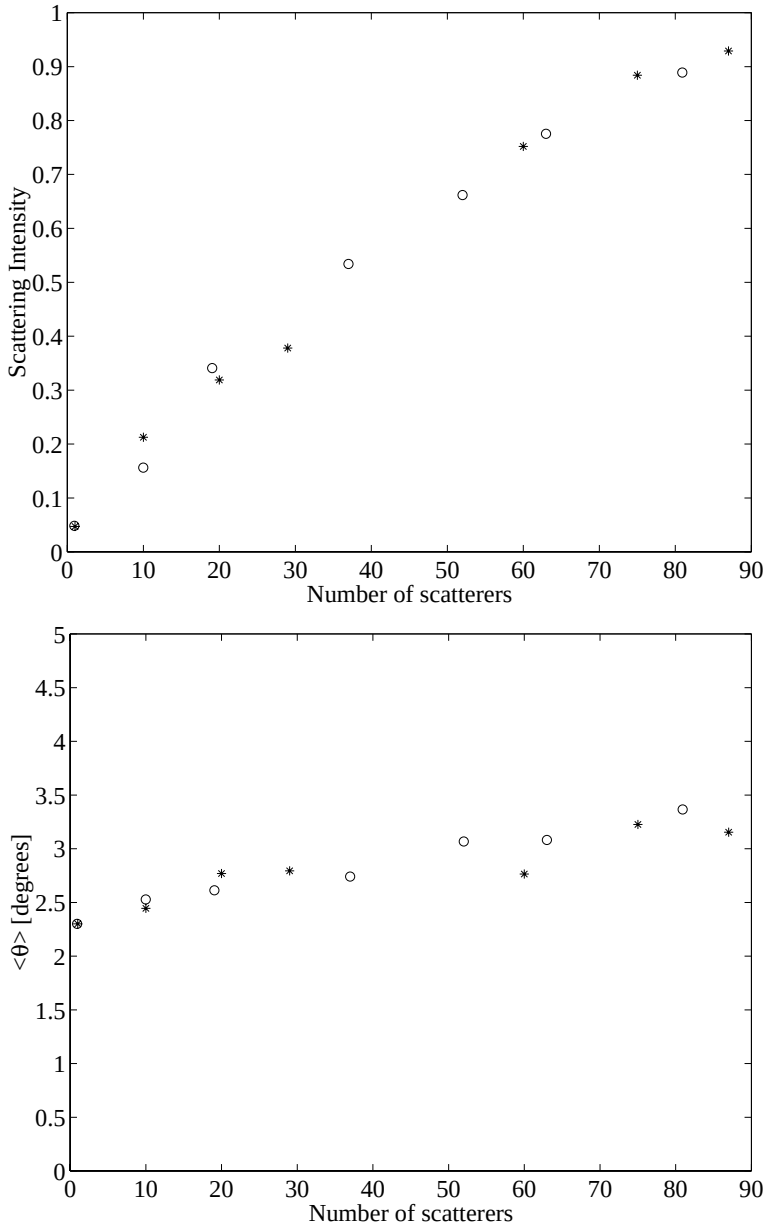


***Figure 8:*** *The dependence of scattered power (top) and the average scattering angle (bottom) on the number of scattering objects. The width of the simulation region is* 160 *μm, while the length of the simulation region is either* $L_x = 160$ *μm (○) or* $L_x = 320$ *μm (⋆)*

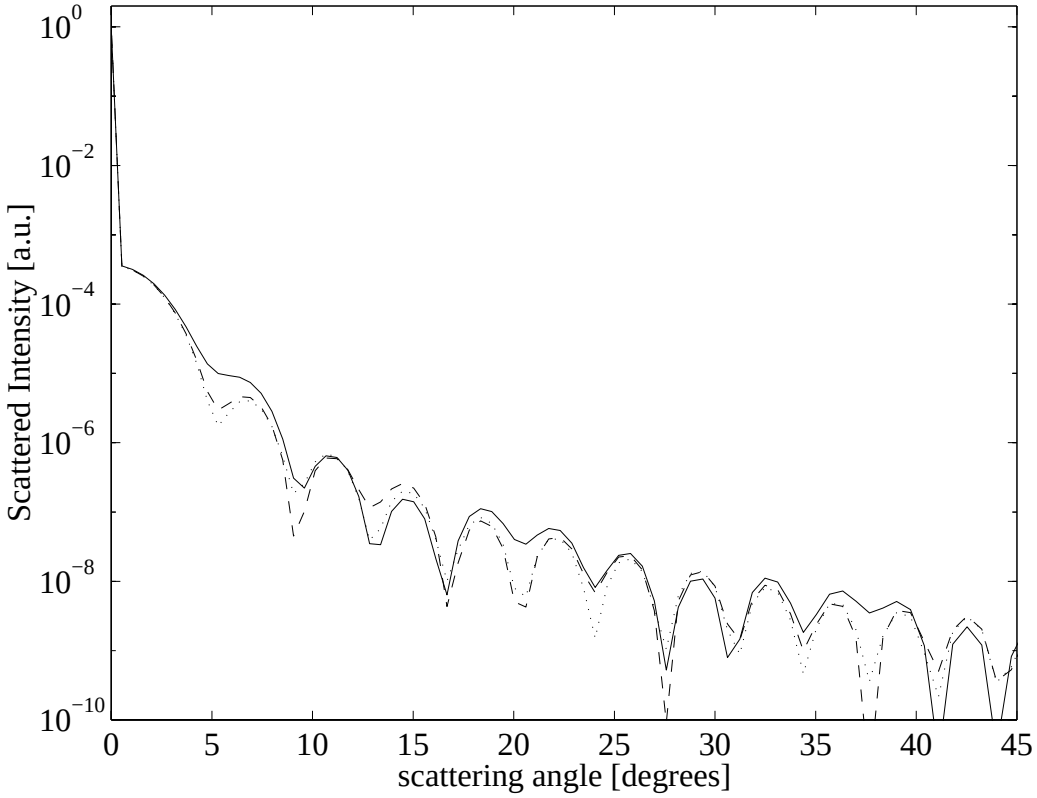


***Figure 9:*** *Scattered light intensity from plane wave for three types of cells : without a nucleus (dotted line), with a small nucleus $D_n = 3$ μm (dashed line), and with a large nucleus $D_n = 6$ μm (solid line). In all 3 cases, the cell diameter $D_0 = 11$ μm.*

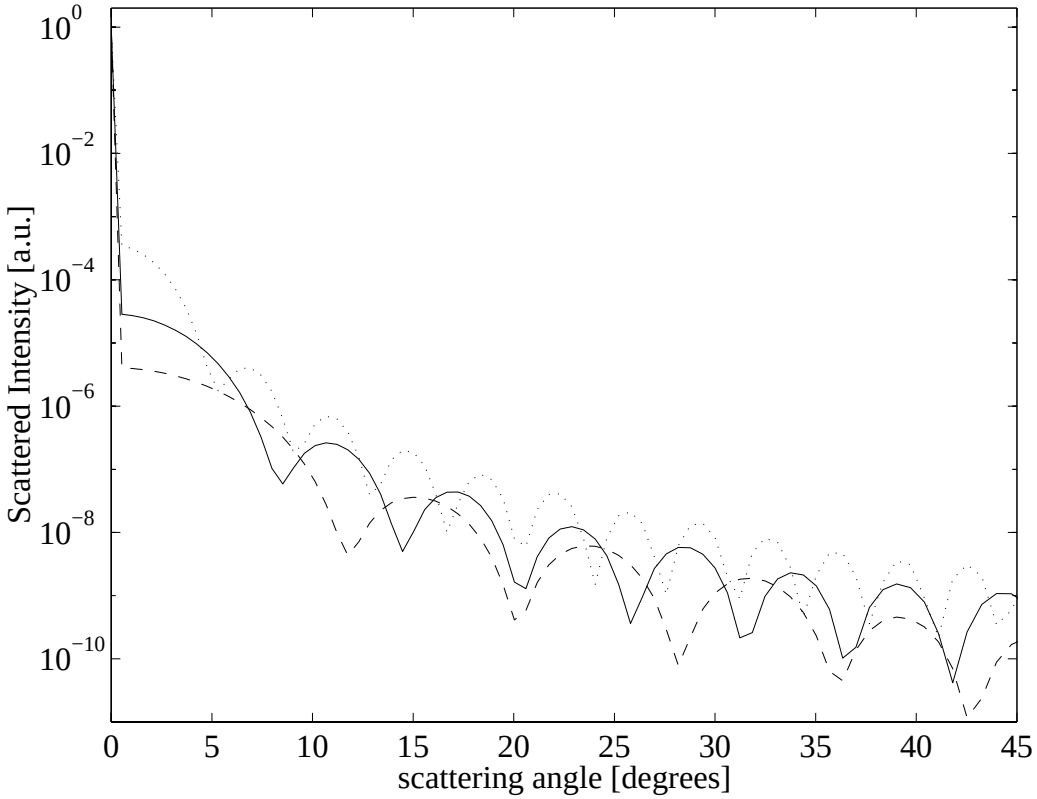


***Figure 10:*** *Scattered light intensity from plane wave for three sizes of cells that do not contain a nucleus : with diameter $D_0 = 11$ µm (dotted line), with diameter $D_0 = 7$ µm (solid line) and with diameter $D_0 = 5$ µm (dashed line).*

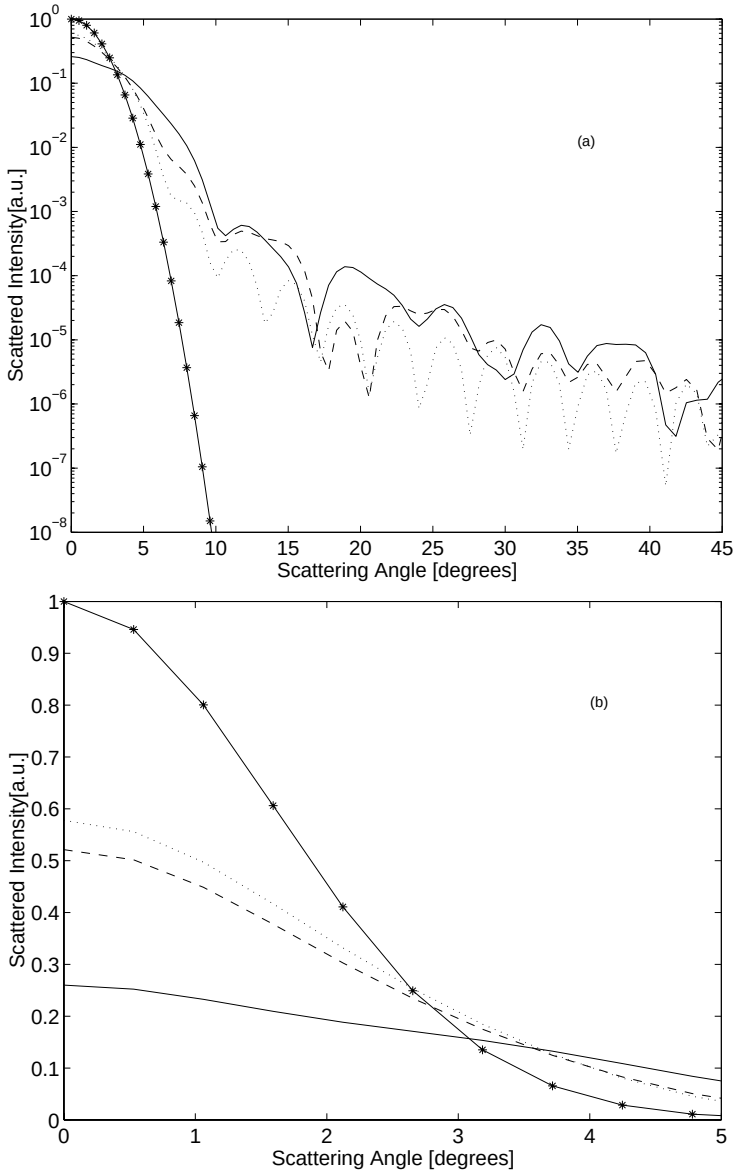


***Figure 11:*** *Scattered intensity from a Gaussian beam with f/3 optics on a logarithmic scale (a) and linear scale (b) for three types of cells: without a nucleus (dotted line), with a small nucleus $D_n = 3$ μm (dashed line), and with a large nucleus $D_n = 6$ μm (solid line). In all cases, the cell diameter is assumed to be $11$ μm and the cell is located in center of the focal spot of the laser beam. The incident beam spectrum is given by the solid lines with the $\star$ symbol.*

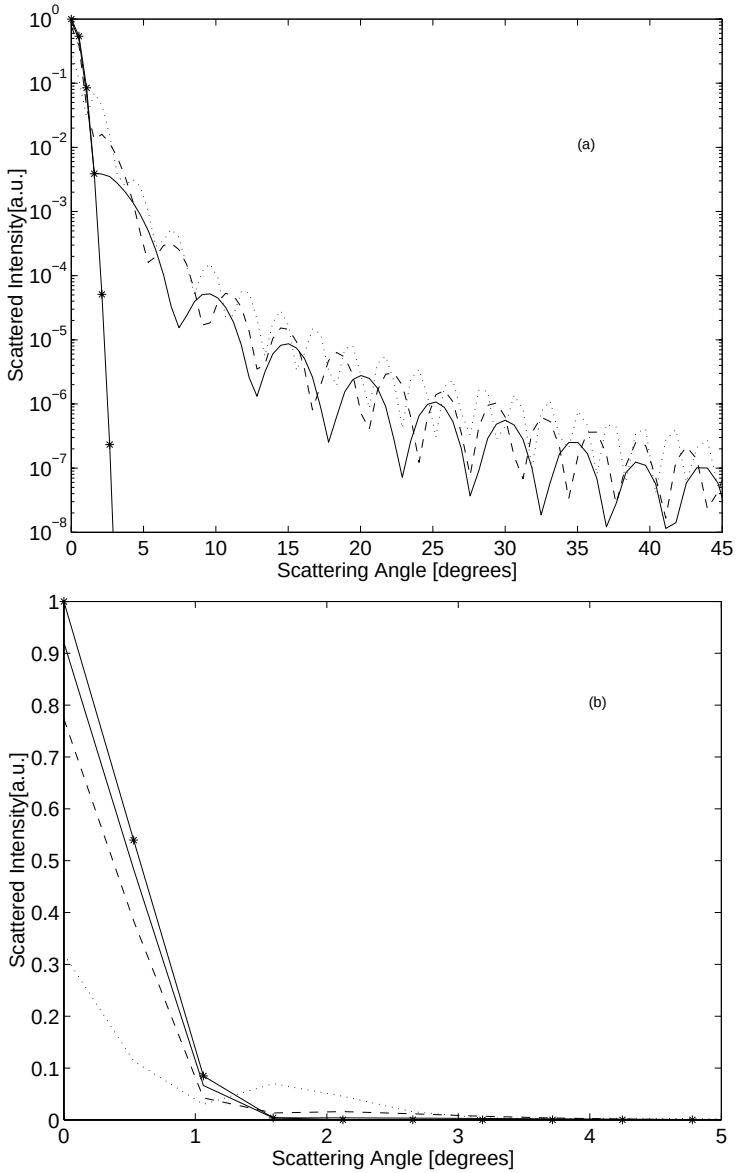


***Figure 12:*** *Scattered intensity from a Gaussian beam with f/10 on a logarithmic scale (a) and linear scale (b) for three types of homogeneous spherical cells of different diameters: with diameter $D_0 = 17$ µm (dotted line), diameter $D_0 = 11$ µm (dashed line), and diameter $D_0 = 8$ µm (solid line). In all cases, the cell is located in center of the focal spot of the laser beam. The incident beam spectrum is given by the solid lines with the $\star$ symbol.*

## DOCUMENT CONTROL DATA

(Security classification of title, body of abstract and indexing annotation must be entered when the overall document is classified)

1. ORIGINATOR (the name and address of the organization preparing the document. Organizations for who the document was prepared, e.g. Establishment sponsoring a contractor's report, or tasking agency, are entered in Section 8.)

Defence R&D Canada – Suffield
P.O. Box 4000, Medicine Hat, AB, Canada T1A 8K6

2. SECURITY CLASSIFICATION (overall security classification of the document, including special warning terms if applicable)

UNCLASSIFIED

3. TITLE (the complete document title as indicated on the title page. Its classification should be indicated by the appropriate abbreviation (S, C or U) in parentheses after the title).

An Approximate Method for Modelling Laser Light Scattering from Biological Cells

4. AUTHORS (Last name, first name, middle initial. If military, show rank, e.g. Doe, Maj. John E.)

Shao, Y. and Yee. E.

5. DATE OF PUBLICATION (month and year of publication of document)

October 2004

6a. NO. OF PAGES (total containing information, include Annexes, Appendices, etc) 45

6b. NO. OF REFS (total cited in document) 33

7. DESCRIPTIVE NOTES (the category of the document, e.g. technical report, technical note or memorandum. If appropriate, enter the type of report, e.g. interim, progress, summary, annual or final. Give the inclusive dates when a specific reporting period is covered.)

Technical Report

8. SPONSORING ACTIVITY (the name of the department project office or laboratory sponsoring the research and development. Include the address.)

Defence R&D Canada – Suffield

9a. PROJECT OR GRANT NO. (If appropriate, the applicable research and development project or grant number under which the document was written. Please specify whether project or grant.)

PCN 16QD40

9b. CONTRACT NO. (If appropriate, the applicable number under which the document was written.)

10a. ORIGINATOR'S DOCUMENT NUMBER (the official document number by which the document is identified by the originating activity. This number must be unique to this document.)

DRDC Suffield TR 2004-187

10b. OTHER DOCUMENT NOs. (Any other numbers which may be assigned this document either by the originator or by the sponsor.)

11. DOCUMENT AVAILABILITY (any limitations on further dissemination of the document, other than those imposed by security classification)

( x ) Unlimited distribution
( ) Distribution limited to defence departments and defence contractors; further distribution only as approved
( ) Distribution limited to defence departments and Canadian defence contractors; further distribution only as approved
( ) Distribution limited to government departments and agencies; further distribution only as approved
( ) Distribution limited to defence departments; further distribution only as approved
( ) Other (please specify):

12. DOCUMENT ANNOUNCEMENT (any limitation to the bibliographic announcement of this document. This will normally corresponded to the Document Availability (11). However, where further distribution (beyond the audience specified in 11) is possible, a wider announcement audience may be selected).

13. ABSTRACT (a brief and factual summary of the document. It may also appear elsewhere in the body of the document itself. It is highly desirable that the abstract of classified documents be unclassified. Each paragraph of the abstract shall begin with an indication of the security classification of the information in the paragraph (unless the document itself is unclassified) represented as (S), (C) or (U). It is not necessary to include here abstracts in both official languages unless the text is bilingual).

A new technique for approximating the scattering of laser light by biological cells is reported. This technique is based on a three-dimensional scalar wave equation approximation of the full Maxwell's field equations for the electromagnetic field. This scalar wave equation for describing the light scattering patterns of cells containing arbitrary morphological structure (e.g., various organelles) is solved numerically using a spectral method. The accuracy of the spectral numerical method is verified by comparison with solutions obtained from linear perturbation theory and Mie theory. Comparison with Mie theory shows that the three-dimensional scalar wave equation is a good approximation to the full Maxwell's field equations for light scattering up to moderate forward scattering angles (i.e., for scattering angles less than about 35°). The approximate technique used here is capable of correctly predicting the scattered intensity patterns from biological cells over a dynamic range spanning six orders of magnitude. The new technique can be applied to calculate the light scattering either from an individual biological cell and from a sample containing an ensemble of such biological cells. The scattering intensity patterns predicted using the new technique can potentially be applied to diagnose the size and internal structure of biological cells, making it a valuable interpretative tool in flow cytometry (e.g., in the detection of rare event cells such as those resulting from a biological warfare agent attack, or for the rapid noninvasive optical assessment of tissue pathology in the detection of cancerous cells).

14. KEYWORDS, DESCRIPTORS or IDENTIFIERS (technically meaningful terms or short phrases that characterize a document and could be helpful in cataloguing the document. They should be selected so that no security classification is required. Identifies, such as equipment model designation, trade name, military project code name, geographic location may also be included. If possible keywords should be selected from a published thesaurus, e.g. Thesaurus of Engineering and Scientific Terms (TEST) and that thesaurus-identified. If it is not possible to select indexing terms which are Unclassified, the classification of each should be indicated as with the title.)

light scattering
biological cells
spectral method
lasers